POLITECNICO DI MILANO
Master's Degree in Computer Science and Engineering
Dipartimento di Elettronica, Informazione e Bioingegneria

DEEP FEATURE EXTRACTION FOR SAMPLE-EFFICIENT REINFORCEMENT LEARNING

Supervisor: Prof. Marcello Restelli
Co-supervisors: Dott. Carlo D'Eramo, Dott. Matteo Pirotta

Master's Thesis by:
Daniele Grattarola (Student ID 853101)

Academic Year 2016-2017

Il più è fatto.

Contents

List of Figures

List of Tables

List of Algorithms

Abstract

Deep reinforcement learning (DRL) has been under the spotlight of artificial intelligence research in recent years, enabling reinforcement learning agents to solve control problems that were previously considered intractable. The most effective DRL methods, however, require a great amount of training samples (in the order of tens of millions) in order to learn good policies even on simple environments, making them a poor choice in real-world situations where the collection of samples is expensive.

In this work, we propose a sample-efficient DRL algorithm that combines unsupervised deep learning to extract a representation of the environment, and batch reinforcement learning to learn a control policy using this new state space. We also add an intermediate step of feature selection on the extracted representation in order to reduce the computational requirements of our agent to the minimum. We test our algorithm on the Atari games environments, and compare the performance of our agent to that of the DQN algorithm by Mnih et al. (2015) [32]. We show that even if the final performance of our agent amounts to a quarter of DQN's, we are able to achieve good sample efficiency and a better performance on small datasets.

Riassunto

L'apprendimento profondo per rinforzo (in inglese *deep reinforcement learning* - DRL) è recentemente diventato il centro dell'attenzione nel campo dell'intelligenza artificiale, per la sua capacità senza precedenti nel risolvere problemi di controllo considerati fino ad ora inavvicinabili. A partire dalla pubblicazione dell'algoritmo *deep Q-learning* (DQN) di Mnih et al. [32], il campo dell'apprendimento per rinforzo ha vissuto un vero e proprio rinascimento, caratterizzato da un susseguirsi di pubblicazioni con algoritmi di controllo sempre più efficaci nel risolvere ambienti ad alta dimensionalità, con prestazioni simili o superiori agli esseri umani. Tuttavia, una caratteristica comune agli algoritmi di DRL è la necessità di utilizzare un enorme numero di campioni di addestramento per arrivare a convergenza. Alcune delle pubblicazioni più recenti cercano di affrontare la problematica, riuscendo però ad abbassare questo numero al massimo di un ordine di grandezza.

Lo scopo di questa tesi è presentare un algoritmo di DRL che riesca ad apprendere politiche di controllo soddisfacenti in ambienti complessi, utilizzando solo una frazione dei campioni necessari agli algoritmi dello stato dell'arte. Il nostro agente utilizza l'apprendimento profondo non supervisionato per estrarre una rappresentazione astratta dell'ambiente, e l'apprendimento per rinforzo in modalità *batch* per ricavare una politica di controllo a partire da questo nuovo spazio degli stati. Aggiungiamo, inoltre, una procedura di selezione delle *feature* applicata alla rappresentazione estratta dall'ambiente, in modo da ridurre al minimo i requisiti computazionali del nostro agente.

In fase sperimentale, applichiamo il nostro algoritmo ad alcuni ambienti di test dei sopracitati giochi Atari, confrontandolo con le prestazioni di DQN. Come risultato principale, mostriamo che il nostro agente è in grado di raggiungere in media un quarto dei punteggi ottenuti da DQN sugli stessi ambienti, ma utilizzando circa un centesimo dei campioni di addestramento. Mostriamo inoltre che, a parità di campioni raccolti dal nostro algoritmo per raggiungere le migliori prestazioni, i punteggi ottenuti dal nostro agente sono in media otto volte più alti di quelli di DQN.

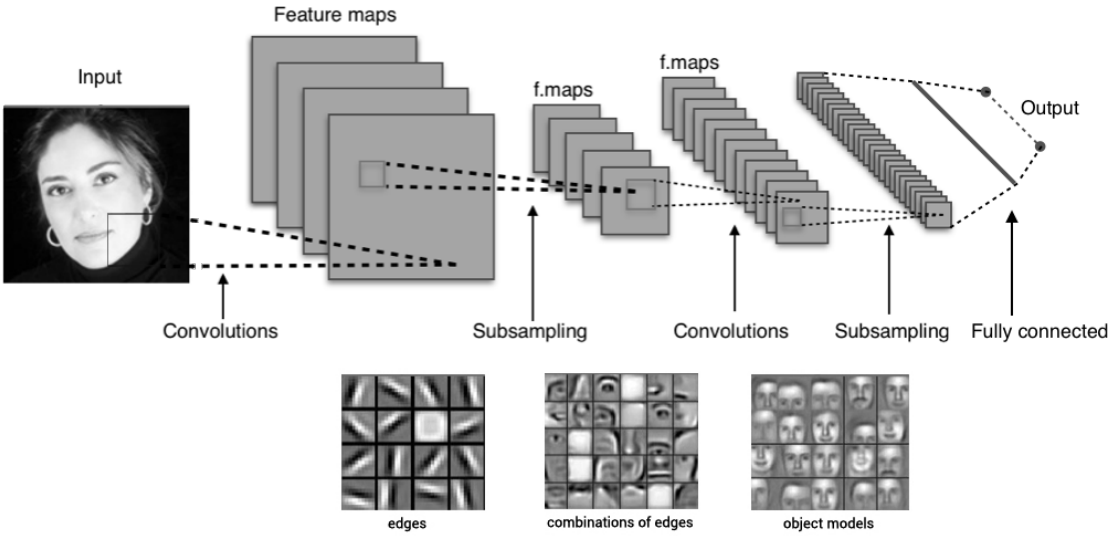

Figura 1: Esempio di estrazione gerarchica di feature con una CNN.

Apprendimento Profondo

L'apprendimento profondo (normalmente noto con il termine inglese *deep learning*) è una tecnica di apprendimento automatico utilizzata per estrarre rappresentazioni astratte del dominio. I metodi profondi si basano su molteplici livelli di rappresentazione, ottenuti dalla composizione di moduli semplici, ma non lineari, che trasformano la rappresentazione ricevuta in ingresso in una rappresentazione leggermente più astratta.

Il deep learning è alla base della ricerca moderna in apprendimento automatico, ed i risultati più impressionanti sono stati tipicamente raggiunti grazie alla versatilità delle reti neurali. Oltre ad essere un potente approssimatore universale, questo semplice modello ispirato alla struttura interconnessa del cervello animale si presta alla composizione gerarchica, rendendolo un blocco ideale per l'apprendimento profondo. Gran parte dei progressi nel campo del deep learning sono dovuti alle reti neurali convoluzionali (in inglese *convolutional neural networks* - CNN), ispirate al funzionamento della corteccia visiva del cervello (Figura 1). Le CNN sono state applicate con notevole successo a svariati problemi, dalla visione artificiale [26, 42] alla traduzione automatica [48], e si basano sull'utilizzo di *filtri* che vengono fatti scorrere sull'ingresso ad ogni livello, per individuare correlazioni spaziali locali che caratterizzino il dominio. L'efficacia delle CNN deriva proprio da questa natura intrinsecamente spaziale, che consente di processare domini complessi (come le immagini) con un'ottima generalità.

Deep Reinforcement Learning

Il deep reinforcement learning (DRL) è una branca dell'apprendimento per rinforzo che utilizza approssimatori ad apprendimento profondo per estrarre una rappresentazione astratta dell'ambiente, e utilizza poi questa rappresentazione per apprendere una politica di controllo ottimale. Il DRL ha causato una vera e propria rivoluzione nel campo dell'intelligenza artificiale, e la letteratura sulla materia ha visto un incremento esponenziale delle pubblicazioni. Tra queste, citiamo nuovamente l'algoritmo che ha innescato l'interesse nel DRL, DQN di Mnih et al. [32], e i derivati di DQN proposti da Van Hasselt et al. (2016) [20] con *Double DQN* (DDQN), Schaul et al. (2016) [38] con *prioritized experience replay* e Wang et al. (2016) [45] con *dueling architecture*. Altri approcci proposti nella letteratura di DRL includono l'algoritmo *Asynchronous Advantage Actor-Critic* (A3C) di Mnih et al. (2016) [31] caratterizzato da un'ottima velocità di apprendimento, il programma *AlphaGo* di Silver et al. (2016) [39] in grado di sconfiggere il campione del mondo Ke Jie nel complicato gioco da tavolo del *Go*, e *Neural Episodic Control* di Pritzel et al. (2017) [36], che al momento della stesura di questa tesi costituisce lo stato dell'arte per l'apprendimento sui famosi ambienti *Atari games*.

La tipica applicazione del DRL consiste nel risolvere problemi di controllo a partire dalla rappresentazione visiva dell'ambiente. Questa configurazione consente di sfruttare l'enorme capacità descrittiva delle CNN e permette di affrontare problemi complessi senza la necessità di ingegnerizzare i descrittori dell'ambiente.

Feature Profonde per l'Apprendimento Efficiente

Come argomento centrale di questa tesi presentiamo un algoritmo di deep reinforcement learning che combina:

- l'apprendimento profondo non supervisionato per estrarre una rappresentazione dell'ambiente;
- un algoritmo per la selezione di feature orientato al controllo, per ridurre al minimo i requisiti computazionali dell'agente;
- un algoritmo di apprendimento automatico in modalità *batch*, per apprendere una politica a partire dalla rappresentazione prodotta dagli altri due moduli.

Lo scopo principale della procedura presentata è quello di apprendere una politica di controllo efficace su un ambiente complesso, utilizzando il minor numero possibile di campioni di addestramento.

Per l'estrazione di feature dall'ambiente, utilizziamo un *autoencoder* convoluzionale (AE). L'AE è una forma di rete neurale che viene utilizzata per apprendere una rappresentazione del dominio in maniera non supervisionata, costituita da due moduli separati:

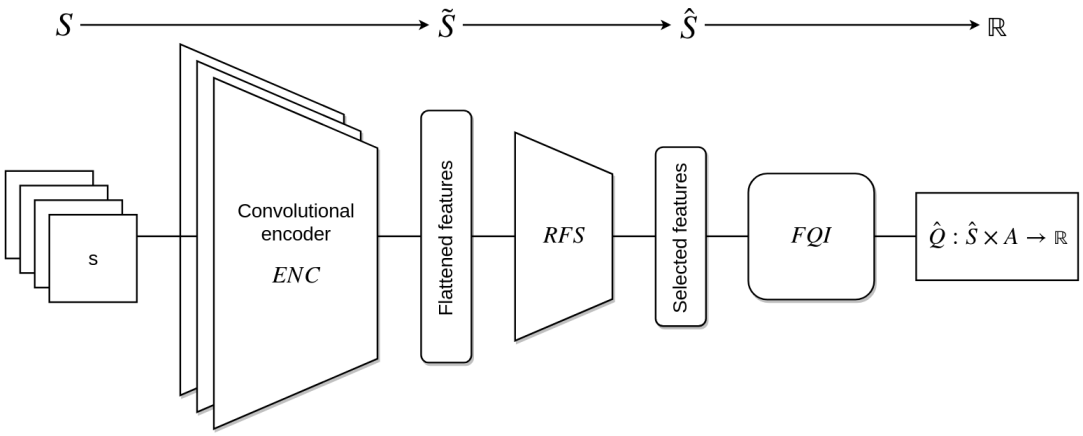

Figura 2: Rappresentazione schematica della composizione dei tre moduli, con le rispettive trasformazioni evidenziate in alto.

un *encoder* e un *decoder*. Lo scopo dell'encoder è semplicemente quello di estrarre una rappresentazione compressa degli ingressi, mentre quello del decoder è di invertire questa trasformazione e ricostruire l'ingresso originale a partire dalla compressione dell'encoder. I due componenti vengono addestrati come un'unica rete neurale, propagando il gradiente su tutti i pesi contemporaneamente. Al termine dell'apprendimento, l'encoder viene utilizzato per comprimere gli elementi del dominio in maniera tale che contengano sufficiente informazione affinchè il decoder possa ricostruirli, idealmente implementando una forma di compressione senza perdita che riduca la dimensionalità dello spazio di ingresso. Identifichiamo questa compressione come la trasformazione $ENC : S \to \tilde{S}$, dallo spazio degli stati originali S, allo spazio delle feature astratte $\tilde{S}$.

Il secondo modulo della nostra catena di addestramento è l'algoritmo *Recursive Feature Selection* di Castelletti et al. [8]. Questa procedura di selezione delle feature utilizza l'apprendimento supervisionato per ordinare le feature di stato di un ambiente in base alla loro utlità per il controllo, e riduce la dimensionalità del dominio rimuovendo le feature meno utili a questo fine. Nel nostro caso, utilizziamo una versione di RFS basata sugli alberi decisionali per ridurre ulteriormente la rappresentazione estratta dall'AE, in modo da ottenere uno spazio delle feature minimale ed essenziale per il controllo. Anche in questo caso, il prodotto del modulo è una trasformazione $RFS : \tilde{S} \to \hat{S}$, dove $\hat{S}$ identifica lo spazio ridotto.

Infine, utilizziamo l'algoritmo di apprendimento automatico batch *Fitted Q-Iteration* (FQI) [11] per apprendere una politica di controllo per l'ambiente a partire da una raccolta di transizioni (s, a, r, s') (*stato, azione, rinforzo, stato prossimo*) dove $s, s' \in \hat{S}$. Alla fine dell'addestramento, l'algoritmo produce un approssimatore della funzione di valore di azione $\hat{Q} : \hat{S} \times A \to \mathbb{R}$, dove A è lo spazio delle azioni.

I tre moduli vengono addestrati in sequenza per produrre le rispettive trasformazioni,

e alla fine della fase di addestramento vengono combinati per poter utilizzare la funzione $\hat{Q}$ prodotta da FQI a partire dallo spazio degli stati originale (Figura 2). La sequenza di addestramento, poi, viene ripetuta all'interno di un ciclo principale, che sequenzialmente raccoglie un insieme di campioni su cui addestrare i tre moduli, utilizzando una politica a tasso di esplorazione decrescente in modo da sfruttare sempre di più la conoscenza appresa dall'agente, fino a convergenza. Ogni sequenza di addestramento è seguita da una fase di valutazione, per stabilire se le prestazioni dell'agente siano soddisfacenti ed eventualmente terminare la procedura.

Esperimenti e Conclusioni

Nella fase sperimentale applichiamo l'algoritmo a tre ambienti dei giochi Atari, e per valutare le prestazioni del nostro agente le compariamo a quelle ottenute da DQN di Mnih et al. [32] sugli stessi giochi.

Osserviamo che l'AE riesce ad ottenere un'ottima precisione nella ricostruzione dello spazio originale degli stati, e che le feature estratte dall'encoder sono sufficientemente astratte. Per verificare la bontà delle feature al fine del controllo, addestriamo un modello supervisionato per approssimare la funzione Q appresa da DQN, a partire dalle feature prodotte dall'AE. L'alto coefficiente di correlazione dei valori predetti in validazione conferma che le feature estratte sono adatte al controllo, o che quantomeno contengono tutta l'informazione necessaria a stimare le funzioni di valore ottime dell'ambiente.

A causa degli enormi requisiti di potenza computazionale, possiamo condurre pochi esperimenti relativi a RFS, e siamo costretti a rimuoverlo completamente dalla catena di addestramento per valutare le prestazioni finali dell'agente in tempi trattabili. I tre esperimenti che portiamo a termine (uno per ogni ambiente), producono risultati variabili e inaspettati, e ci portano a rimandare l'analisi della procedura di selezione ad un secondo momento.

Infine, la valutazione dell'algoritmo completo conferma il raggiungimento dell'obiettivo di efficienza e sottolinea un grande potenziale della procedura, che tuttavia non riesce ad arrivare alle stesse prestazioni dello stato dell'arte. Il nostro agente riesce ad ottenere in media il 25% del punteggio di DQN, utilizzando però lo 0.4% dei campioni di addestramento richiesti in media da DQN per raggiungere la miglior prestazione. Allo stesso tempo, valutando i punteggi raggiunti da entrambi gli algoritmi limitandosi a questo numero di campioni estremamente ridotto, osserviamo che il nostro agente ottiene punteggi mediamente superiori di otto volte rispetto a quelli di DQN, che necessita di un numero dieci volte più grande di esempi per imparare una politica equivalente. Il nostro algoritmo dimostra dunque una grande efficienza nell'utilizzo dei campioni, rendendolo adatto al controllo in situazioni in cui la raccolta di campioni è difficile o costosa.

Acknowledgments

All the work presented in this thesis was done under the supervision of Prof. Marcello Restelli, who has instilled in me the passion for this complex and fascinating subject and helped me navigate it since the beginning. I also thank Dott. Carlo D'Eramo for guiding me during my first steps into the academic world and inspiring me to pursue a career in research, and Dott. Matteo Pirotta for providing useful insights and supervision on this work.

It is impossible to summarize the unique experience I had at PoliMi in a few paragraphs, but I would like to thank Ilyas Inajjar, Giacomo Locci, Angelo Gallarello, Davide Conficconi, Alessandro Comodi, Francesco Lattari, Edoardo Longo, Stefano Longari, Yannick Giovanakis, Paolo Mosca and Andrea Lui for sharing their experiences with me and always showing me a different perspective of the things we do. I thank Politecnico di Milano for providing the infrastructure during my education and the writing of this thesis, but most importantly for fostering a culture of academic excellence, of collaboration, and of passion for the disciplines of its students. I also thank Prof. Cremonesi and Prof. Alippi for giving me a chance to prove myself.

Finally, this thesis is dedicated to my parents, for giving me all that I am and all that I have; to Gaia, for being the reason to always look ahead; to my grandmothers, for their unconditional love; to my grandfather, for always rooting silently.

Chapter 1

Introduction

Human behavior is a complex mix of elements. We are subject to well defined biological and social forces, but at the same time our actions are deliberate, our thinking is abstract, and our objectives can be irrational; our brains are extremely complex interconnections, but of extremely simple building blocks; we are crafted by ages of random evolution, but at the same time of precise optimization. When we set out to describe the inner workings of human cognition, we must consider all of these colliding aspects and account for them in our work, without overcomplicating what is simple or approximating what is complex.

Artificial intelligence is a broad field, that looks at the variegate spectrum of human behavior to replicate our complexity in a formal or algorithmic way. Among the techniques of AI, one family of algorithms called *machine learning* is designed to give computers the ability to *learn* to carry out a task without being explicitly programmed to do so. The focus on different types of tasks is what defines the many subfields of machine learning. For instance, the use of machine learning algorithms to take decisions in a *sequential decision-making problem* is called *reinforcement learning*, whereas *deep learning* is a family of techniques to learn an abstract representation of a vector space (e.g. learning how to describe an image from the value of its pixels).

Teaching machines to behave like human beings is a complex and inspiring problem on its own; however, an even more complex task is not to simply teach computers to mimic humans, but to do so with the same learning *efficiency* of the biological brain, which is able to solve problems by experiencing them very few times (sometimes even imagining a problem is enough to solve it, by comparing it with other similar known situations). The purpose of this thesis is to make a step in this direction by combining powerful machine learning techniques with efficient ones, in order to tackle complex control problems without needing many examples to learn from.

1.1 Goals and Motivation

The source of inspiration for this work comes from the recent progress in reinforcement learning associated to *deep reinforcement learning* (DRL) techniques. Among these, we cite *Deep Q-Learning* by Mnih et al. [32], the *Asynchronous Advantage Actor-Critic* algorithm also by Mnih et al. [31], and the *Neural Episodic Control* algorithm by Pritzel et al. [36]. All these algorithms (which were all the state of the art at the time of their respective publication), are based on deep learning to extract the visual characteristics of an environment, and then using those characteristics to learn a policy with well-known reinforcement learning techniques. A major drawback of these approaches, however, is that they all require an enormous amount of experience to converge, which may prove unfeasible in real-world problems where the collection of examples is expensive. The main purpose of this work is to explore the limits of this apparent requirement, and to propose an algorithm that is able to perform well even under such scarcity conditions.

1.2 Proposed Solution

We introduce a deep reinforcement learning agent that extracts an abstract description of the environment starting from its visual characteristics, and then leverages this description to learn a complex behavior using a small collection of training examples.

We devise a combination of different machine learning techniques. We use *unsupervised* deep learning to extract a representation of the visual characteristics of the environment, as well as a *feature selection* procedure to reduce this representation while keeping all the necessary information for control, and a *batch* reinforcement learning algorithm which exploits this filtered representation to learn a *policy*. The result is a reinforcement learning procedure that requires a small amount of experience in order to learn, and which produces an essential and general representation of the environment as well as a well-performing control policy for it.

We test our algorithm on the *Atari games* environments, which are the *de facto* standard test bench of deep reinforcement learning, and we also perform an experimental validation of all the components in our learning pipeline in order to ensure the quality of our approach. We test the suitability of the extracted representation to both describe the environment and provide all the information necessary for control, as well as we gain useful knowledge on some environments by looking at the feature selection.

We compare our results with the DQN algorithm by Mnih et al. [32], and we find that our agent is able to learn non-trivial policies on the tested environments, but that it fails to converge to the same performance of DQN. However, we show that the number of samples required by our procedure to reach its maximum performance is up to two orders of magnitude smaller than that required by DQN, and that our agent's performance is on average eight times higher when limiting the training of the two methods to this

small number of samples.

1.3 Original Contributions

The use of unsupervised deep learning to extract a feature space for control purposes had already been proposed by Lange and Riedmiller [27] before the field of deep reinforcement learning really took off in the early 2010s. However, their approach used a different architecture for the feature extraction, which would be inefficient for complex control problems like the ones we test in this work.

Moreover, to the best of our knowledge there is no work in the literature that applies a feature selection technique to deep features explicitly targeted for control purposes. This additional step allows us to optimize our feature extraction process for obtaining a generic description of the environment rather than a task-specific one, while at the same time improving the computational requirements of our agent by keeping only the essential information.

Our algorithm makes a step towards a more sample-efficient deep reinforcement learning, and would be a better pick than DQN in situations characterized by a lack of training samples and a big state space.

1.4 Thesis Structure

The thesis is structured as follows.

In Chapter 2 we provide the theoretical framework on which our algorithm is based, and we give an overview of the most important concepts and techniques in the fields of deep learning and reinforcement learning.

In Chapter 3 we summarize the state-of-the-art results in the field of deep reinforcement learning.

In Chapter 4 we introduce our deep reinforcement learning algorithm, and provide a formal description of its components and their behavior.

In Chapter 5 we describe in detail the specific implementation of each module in the algorithm, with architectural choices, model hyperparameters, and training configurations.

In Chapter 6 we show experimental results from running the algorithm on different environments.

In Chapter 7 we summarize our work and discuss possible future developments and improvements.

Chapter 2

Background

In this chapter we outline the theoretical framework that will be used in the following chapters. The approach proposed in this thesis draws equally from the fields of *deep learning* and *reinforcement learning*, in a hybrid setting usually called *deep reinforcement learning*.

In the following sections we give high level descriptions of these two fields, in order to introduce a theoretical background, a common notation, and a general view of some of the most important techniques in each area.

2.1 Deep Learning

Deep Learning (DL) is a branch of machine learning that aims to learn abstract representations of the input space by means of complex function approximators. Deep-learning methods are based on multiple levels of representation, obtained by composing simple but nonlinear modules that each transform the representation at one level (starting with the raw input) into a representation at a higher, slightly more abstract level [28].

Deep learning is at the heart of modern machine learning research, where deep models have revolutionized many fields like computer vision [26, 42], machine translation [48] and speech synthesis [44]. Generally, the most impressive results of deep learning have been achieved through the versatility of *neural networks*, which are universal function approximators well suited for hierarchical composition.

In this section we give a brief overview of the basic concepts behind *deep neural networks* and introduce some important ideas that will be used in later chapters of this thesis.

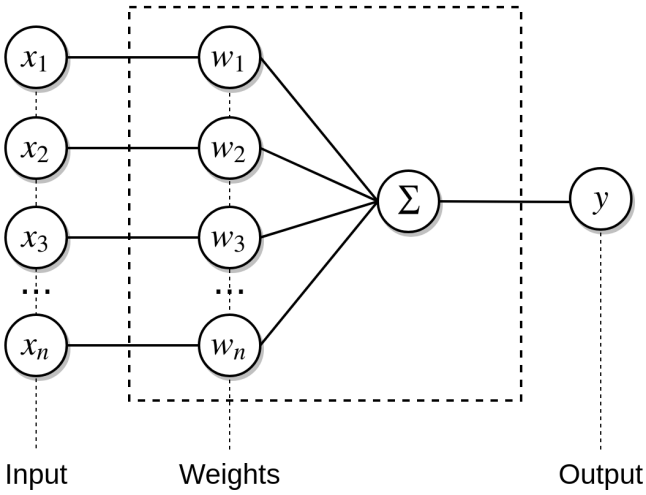

Figure 2.1: Graphical representation of the perceptron model.

2.1.1 Artificial Neural Networks

Feed-forward Artificial Neural Networks (ANNs) [5] are universal function approximators inspired by the connected structure of neurons and synapses in biological brains. ANNs are based on a fairly simple computational model called *perceptron* (Figure 2.1), which is a transformation of an n-space into a scalar value

$$z = \sum_{i=1}^{n} (w_i \cdot x_i) + b \tag{2.1}$$

where $x = (x_1, ..., x_n)$ is the n-dimensional input to the model, $w = (w_1, ..., w_n)$ is a set of weights associated to each component of the input, and b is a bias term (in some notations the bias is embedded in the transformation by setting $x_0 = 1$ and $w_0 = b$).

In ANNs, the simple model of the perceptron is used to create a layered structure, in which each *hidden* layer is composed by a given number of perceptrons (called *neurons*) that (see Figure 2.2):

1. take as input the output of the previous layer;
2. are followed by a nonlinearity σ called the *activation function*;
3. output their value as a component of some m-dimensional space which is the input space of the following layer.

In simpler terms, each hidden layer computes an affine transformation of its input space:

$$z^{(i)} = W^{(i)} \cdot \sigma(z^{(i-1)}) + B^{(i)} \tag{2.2}$$

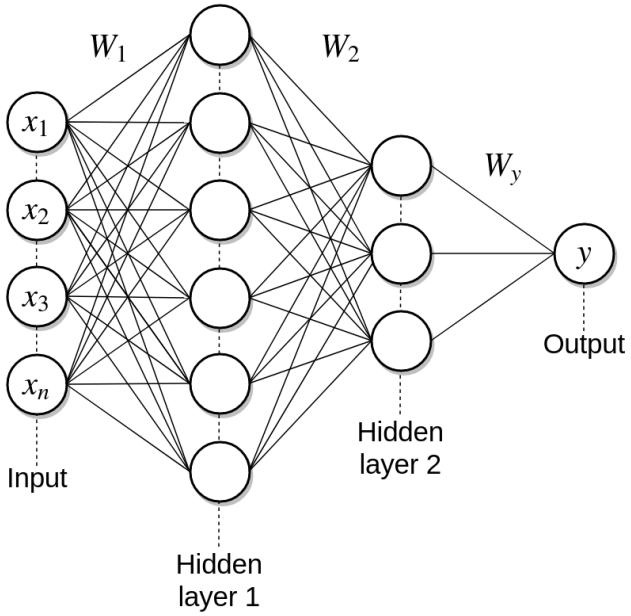

Figure 2.2: A fully-connected neural network with two hidden layers.

where $W^{(i)}$ is the composition of the weights associated to each neuron in the layer and B is the equivalent composition of the biases.

The processing of the input space performed by the sequence of layers that compose an ANN is equivalent to the composition of multiple nonlinear transformations, which results in the production of an output vector on the co-domain of the target function.

2.1.2 Backpropagation

Training ANNs is a parametric learning problem, where a *loss* function is minimized starting from a collection of *training samples* collected by the real process which is being approximated. In parametric learning the goal is to find the optimal parameters of a mathematical model, such that the expected error made by the model on the training samples is minimized. In ANNs, the parameters that are optimized are the weight matrices $W^{(i)}$ and biases $B^{(i)}$ associated to each hidden layer of the network.

In the simple perceptron model, which basically computes a linear transformation of the input, the optimal parameters are learned from the training set according to the following *update rule*:

$$w_i^{new} = w_i^{old} - \eta(\hat{y} - y)x_i, \forall i = (1, ..., n) \tag{2.3}$$

where $\hat{y}$ is the output of the perceptron, y is the real target from the training set, x_i is the i-th component of the input, and η is a scaling factor called the *learning rate* which regulates how much the weights are allowed to change in a single update. Successive

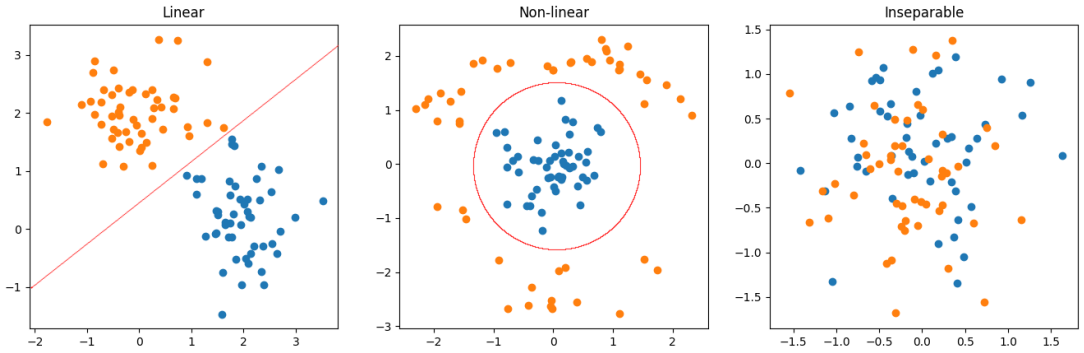

Figure 2.3: Different classification problems on a two-dimensional space, respectively linearly, non-linearly and non separable. The perceptron would be able to converge and correctly classify the points only in the first setting.

applications of the update rule for the perceptron guarantee convergence to an optimum if and only if the approximated function is linear (in the case of regression) or the problem is linearly separable (in the case of classification) as shown in Figure 2.3.

The simple update rule of the perceptron, however, cannot be used to train an ANN with multiple layers because the true outputs of the hidden layers are not known a priori. To solve this issue, it is sufficient to notice that the function computed by each layer of a network is nonlinear, but differentiable with respect to the layer's input (i.e. it is linear in the weights). This simple fact allows to compute the partial derivative of the loss function for each weight matrix in the network to, in a sense, impute the error committed on a training sample proportionally across neurons. The error is therefore propagated backwards (hence the name *backpropagation*) to update all weights in a similar fashion to the perceptron update. The gradient of the loss function is then used to change the value of the weights, with a technique called *gradient descent* which consists in the following update rule:

$$W_i^{new} = W_i^{old} - \eta \frac{\partial L(y, \hat{y})}{\partial W_i^{old}} \tag{2.4}$$

where L is any differentiable function of the target and predicted values that quantifies the error made by the model on the training samples. The term *gradient descent* is due to the fact that the weights are updated in the opposite direction of the loss gradient, moving towards a set of parameters for which the loss is lower (see Figure 2.4).

Notice that traditional gradient descent optimizes the loss function over all the training set at once, performing a single update of the parameters. This approach, however, can be computationally expensive when the training set is big; a more common approach is to use *stochastic gradient descent* (SGD) [5], which instead performs sequential parameters updates using small subsets of the training samples (called *batches*). As the

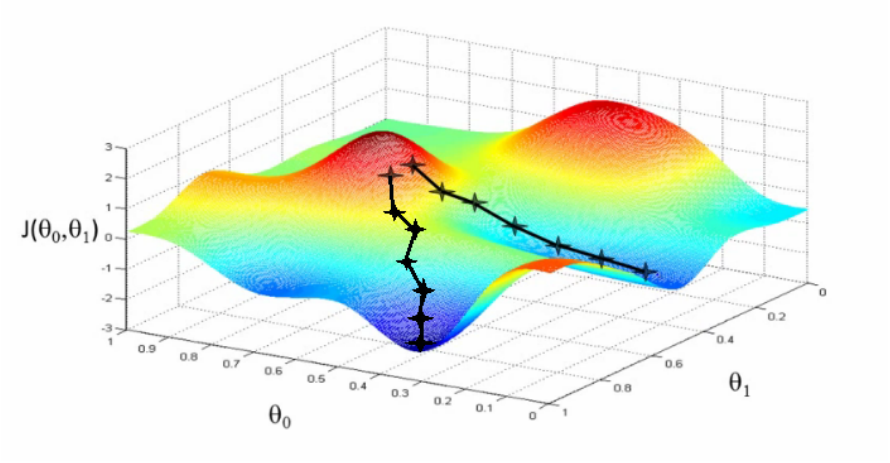

Figure 2.4: Visualization of SGD on a space of two parameters.

number of samples in a batch decreases, the variance of the updates increases, because the error committed by the model on a single sample can have more impact on the gradient step. This can cause the optimization algorithm to *miss* a good local optima due to excessively big steps, but at the same time could help leaving a poor local minimum in which the optimization is stuck. The same applies to the learning rate, which is the other important factor in controlling the size of the gradient step: if the learning rate is too big, SGD can *overshoot* local minima and fail to converge, but at the same time it may take longer to find the optimum if the learning rate is too small (Figure 2.5).

In order to improve the accuracy and speed of SGD, some particular tweaks are usually added to the optimization algorithm. Among these, we find the addition of a *momentum* term to the update step of SGD, in order to avoid oscillating in irrelevant directions by incorporating a fraction of the previous update term in the current one:

$$W_i^{(j+1)} = W_i^{(j)} - \gamma\eta \frac{\partial L(y^{(j-1)}, \hat{y}^{(j-1)})}{\partial W_i^{(j-1)}} - \eta \frac{\partial L(y^{(j)}, \hat{y}^{(j)})}{\partial W_i^{(j)}} \tag{2.5}$$

where (j) is the number of updates that have occurred so far. In this approach, momentum has the same meaning as in physics, like when a body falling down a slope tends to preserve part of its previous velocity when subjected to a force. Other techniques to improve convergence include the use of an adaptive learning rate based on the previous gradients computed for the weights (namely the *Adagrad* [9] and *Adadelta* [49] optimization algorithms), and a similar approach which uses an adaptive momentum term (called *Adam* [25]).

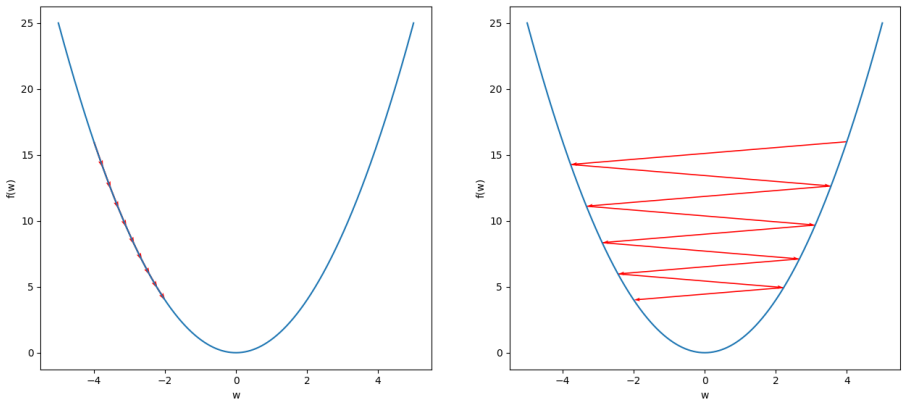

Figure 2.5: Effect of the learning rate on SGD updates. Too small (left) may take longer to converge, too big (right) may overshoot the optimum and even diverge.

2.1.3 Convolutional Neural Networks

Convolutional Neural Networks (CNNs) are a type of ANN inspired by the visual cortex in animal brains, and have been widely used in recent literature to reach state-of-the-art results in fields like computer vision, machine translation, and, as we will see in later sections, reinforcement learning.

CNNs exploit spatially-local correlations in the neurons of adjacent layers by using a *receptive field*, a set of weights which is used to transform a local subset of the input neurons of a layer. The receptive field is applied as a *filter* over different locations of the input, in a fashion that resembles how a signal is *strided* across the other during convolution. The result of this operation is a nonlinear transformation of the input space into a new space (of compatible dimensions) that preserves the spatial information encoded in the input (e.g. from the $n \times m$ pixels of a grayscale image to a $j \times k$ matrix that represents subgroups of pixels in which there is an edge).

While standard ANNs have a *fully connected* (sometimes also called *dense*) structure, with each neuron of a layer connected to each neuron of the previous and following layer, in CNNs the weights are associated to a filter and *shared* across all neurons of a layer, as shown in Figure 2.6. This *weights sharing* has the double advantage of greatly reducing the number of parameters that must be updated during training, and of forcing the network to learn general abstractions of the input that can be applied to any subset of neurons covered by the filter.

In general, the application of a filter is not limited to one per layer and it is customary to have more than one filter applied to the same input in parallel, to create a set of independent abstractions called *feature maps* (also referred to as *channels*, to recall the terminology of RGB images for which a 3-channel representation is used for red, green,

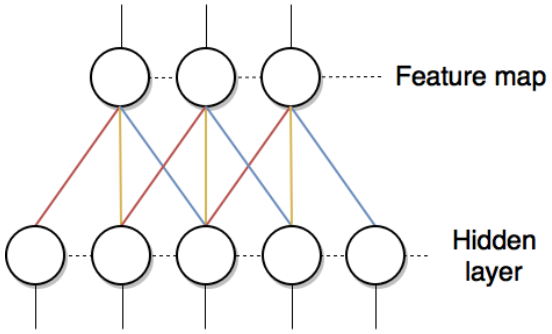

Figure 2.6: Simple representation of shared weights in a 1D CNN. Each neuron in the second layer applies the same receptive field of three weights to three adjacent neurons of the previous layer. The filter is applied with a stride of one element to produce the feature map.

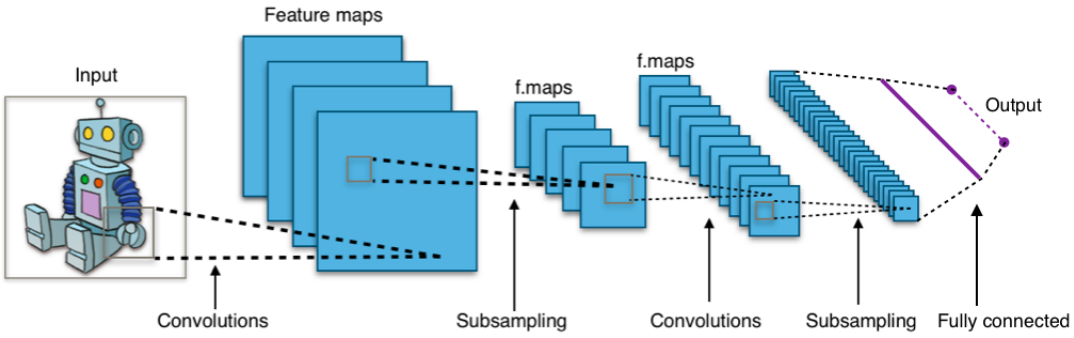

Figure 2.7: Typical structure of a deep convolutional neural network for image processing, with two convolutional hidden layers and a dense section at the end (for classification or regression).

and blue). In this case, there will be a set of shared weights for each filter. When a set of feature maps is given as input to a convolutional layer, a multidimensional filter is strided simultaneously across all channels.

At the same time, while it may be useful to have parallel abstractions of the input space (which effectively enlarges the output space of the layers), it is also necessary to force a reduction of the input in order to learn useful representations. For this reason, convolutional layers in CNNs are often paired with *pooling layers* that reduce the dimensionality of their input according to some criteria applied to subregions of the input neurons (e.g. for each two by two square of input neurons, keep only the maximum activation value as shown in Figure 2.8).

Finally, typical applications of CNNs in the literature use mixed architectures composed of both convolutional and fully connected layers (Figure 2.7). In tasks like image classification [40, 42], convolutional layers are used to extract significant features directly from the images, and dense layers are used as a final classification model; the training in this case is done in an end-to-end fashion, with the classification error being propagated

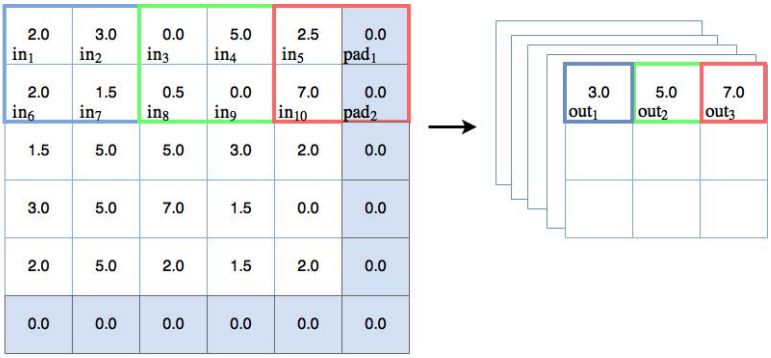

Figure 2.8: Example of max pooling, where only the highest activation value in the pooling window is kept.

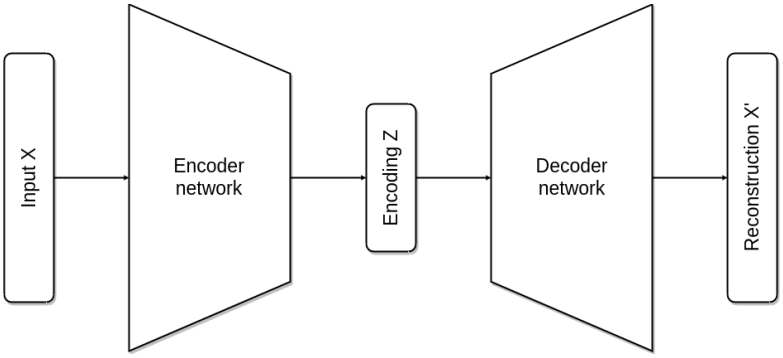

Figure 2.9: Schematic view of an autoencoder, with the two main components represented separately.

across all layers to *fine-tune* all weights and filters to the specific problem.

2.1.4 Autoencoders

Autoencoders (AE) are a type of ANN which is used to learn a sparse and compressed representation of the input space, by sequentially compressing and reconstructing the inputs under some sparsity constraint.

The typical structure of an AE is split into two sections: an *encoder* and a *decoder* (Figure 2.9). In the classic architecture of autoencoders these two components are exact mirrors of one another, but in general the only constraint that is needed to define an AE is that the dimensionality of the input be the same as the dimensionality of the output. In general, however, the last layer of the encoder should output a reduced representation of the input which contains enough information for the decoder to invert the transformation.

The training of an AE is done in an unsupervised fashion, with no explicit target required as the network is simply trained to predict its input. Moreover, a strong

regularization constraint is often imposed on the innermost layer to ensure that the learned representation is as abstract as possible (typically the $L1$ norm of the activations is minimized as additional term to the loss, to enforce sparsity).

Autoencoders can be especially effective in extracting meaningful features from the input space, without tailoring the features to a specific problem like in the end-to-end image classification example of Section 2.1.3 [10]. An example of this is the extraction of features from images, where convolutional layers are used in the encoder to obtain an abstract description of the image's structure. In this case, the decoder uses convolutional layers to transform subregions of the representation, but the expansion of the compressed feature space is delegated to *upscaling layers* (the opposite of pooling layers) [30]. This approach in building the decoder, however, can sometimes cause blurry or inaccurate reconstructions due to the upscaling operation which simply replicates information rather than transforming it (like pooling layers do). Because of this, a more sophisticated technique has been developed recently which allows to build purely convolutional autoencoders, without the need of upscaling layers in the decoder. The layers used in this approach are called *deconvolutional*[1] and are thoroughly presented in [50]. For the purpose of this thesis it suffices to notice that image reconstruction with this type of layer is incredibly more accurate, down to pixel-level accuracy.

2.2 Reinforcement Learning

Reinforcement Learning (RL) is an area of machine learning that studies how to optimize the behavior of an agent in an environment, in order to maximize the cumulative sum of a scalar signal called *reward* in a setting of *sequential decision making*. RL has its roots in optimization and control theory but, because of the generality of its characteristic techniques, it has been applied to a variety of scientific fields where the concept of *optimal behavior in an environment* can be applied (examples include game theory, multi-agent systems and economy). The core aspect of reinforcement learning problems is to represent the setting of an agent performing decisions in an environment, which is in turn affected by the decisions; a scalar reward signal represents a time-discrete indicator of the agent's performance. This kind of setting is inspired to the natural behavior of animals in their habitat, and the techniques used in reinforcement learning are well suitable to describe, at least partially, the complexity of living beings.

In this section we introduce the basic setting of RL and go over a brief selection of the main techniques used to solve RL problems.

[1] Or *transposed convolutions*.

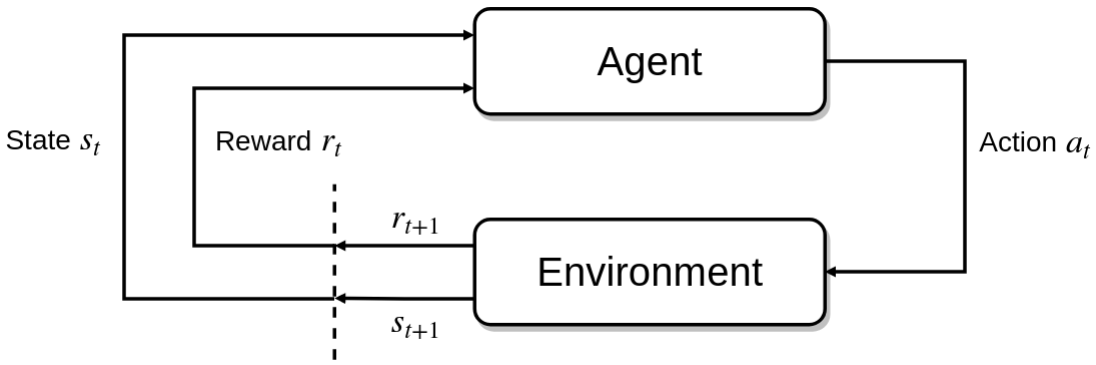

Figure 2.10: The reinforcement learning setting, with the agent performing actions on the environment and in turn observing the state and reward.

2.2.1 Markov Decision Processes

Markov Decision Processes (MDPs) are discrete-time, stochastic control processes, that can be used to describe the interaction of an *agent* with an *environment* (Figures 2.10 and 2.11).

Formally, MDPs are defined as 7-tuples $< S, S^T, A, P, R, \gamma, \mu >$, where:

- S is the set of observable states of the environment. When the set if observable states coincides with the true set of states of the environment, the MDP is said to be *fully observable*. We will only deal with fully observable MDPs without considering the case of *partially observable* MDPs.
- $S^T \subseteq S$ is the set of *terminal states* of the environment, meaning those states in which the interaction between the agent and the environment ends. The sequence of events that occur from when the agent observes an initial state until it reaches a terminal state is usually called *episode*.
- A is the set of actions that the agent can execute in the environment.
- $P : S \times A \times S \rightarrow [0, 1]$ is a *state transition function* which, given two states $s, s' \in S$ and an action $a \in A$, represents the probability of the agent going to state s' by executing a in s.
- $R : S \times A \rightarrow \mathbb{R}$ is a *reward function* which represents the reward that the agent collects by executing an action in a state.
- $\gamma \in [0, 1]$ is a *discount factor* which is used to weight the importance of rewards during time: $\gamma = 0$ means that only the immediate reward is considered, $\gamma = 1$ means that all rewards have the same importance.

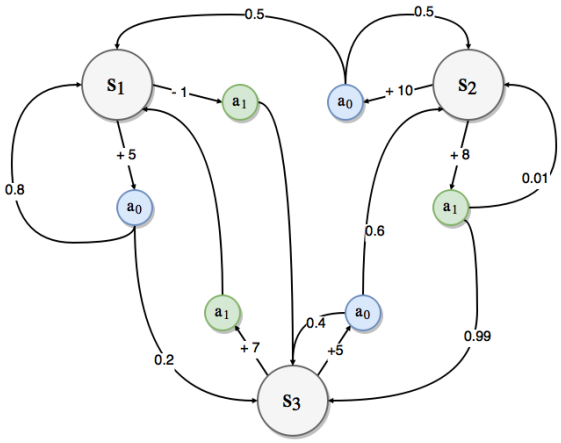

Figure 2.11: Graph representation of an MDP. Each gray node represents a state, each arc leaving a state is associated to an action and its corresponding reward, an the action is in turn associated to the following state; note that actions may have probability distributions over the outgoing arcs.

- $\mu : S \to [0, 1]$ is a probability distribution over S which models the probability of starting an episode in a given state.

Episodes are usually represented as sequences of tuples

$$[(s_0, a_0, r_1, s_1), ..., (s_{n-1}, a_{n-1}, r_n, s_n)]$$

called *trajectories*, where $s_0 \sim \mu$, $s_n \in S^T$, and $(s_i, a_i, r_{i+1}, s_{i+1})$ represents a transition of the agent to state s_{i+1} by taking action a_i in s_i and collecting a reward r_{i+1}.

In MDPs the modeled environment must satisfy the *Markov property*, meaning that the reward and transition functions of the environment must only depend on the current state and action, and not on the past state-action trajectory of the agent. In other words, an environment is said to satisfy the Markov property when its one-step dynamics allow to predict the next state and reward given only the current state and action.

Policy

The behavior of the agent in an MDP can be defined as a probability distribution $\pi : S \times A \to [0, 1]$ called a *policy*, which given $s \in S$ and $a \in A$, represents the probability of selecting a as next action from s. An agent that uses this probability distribution to select its next action when in a given state is said to be *following* the policy.

A common problem when defining policies is the *exploration-exploitation* dilemma. An agent following a policy may end up observing the same trajectories in all episodes (e.g., when following a deterministic policy in a deterministic MDP), but there may be cases in which a better behavior could be had if the agent *explored* other states

instead of simply *exploiting* its knowledge. It is therefore common to add a probabilistic element to policies (irrespectively of their determinism), in order to explicitly control the exploration degree of the agent. Common techniques to control the *exploration-exploitation* trade-off are:

- ε-greedy policies, in which actions are selected using a given policy with probability $1 - \varepsilon$, and randomly the rest of the time;
- softmax action selection, that improves on ε-greedy policies by reducing the number of times a suboptimal action is randomly selected. To do so, a probability distribution (commonly a *Boltzmann distribution*) dependent on the expected return from the successor states (something called the *value* of the states, which we introduce in the next subsection) is used.

Value Functions

Starting from the concept of policy, we can now introduce a function that evaluates how good it is for an agent following a policy π to be in a given state. This evaluation is expressed in terms of the expected return, i.e. the expected discounted sum of future rewards collected by an agent starting from a state while following π, and the function that computes it is called the *state-value function for policy* π (or, more commonly, just *value function*).

Formally, the state-value function associated to a policy π is a function $V^\pi : S \to \mathbb{R}$ defined as:

$$V^\pi(s) = E_\pi[R_t | s_t = s] \tag{2.6}$$

$$= E_\pi[\sum_{k=0}^{\infty} \gamma^k r_{t+k+1} | s_t = s] \tag{2.7}$$

where $E_\pi[\cdot]$ is the expected value given that the agent follows policy π, and t is any time step of an episode $[s_0, ..., s_t, ..., s_n]$ where $s_t \in S, \forall t = 0, ..., n$.

Similarly, we can also introduce a function that evaluates the goodness of taking a specific action in a given state, namely the expected reward obtained by taking an action $a \in A$ in a state $s \in S$ and then following policy π. We call this function the *action-value function for policy* π denoted $Q^\pi : S \times A \to \mathbb{R}$, and defined as:

$$Q^\pi(s, a) = E_\pi[R_t | s_t = s, a_t = a] \tag{2.8}$$

$$= E_\pi[\sum_{k=0}^{\infty} \gamma^k r_{t+k+1} | s_t = s, a_t = a] \tag{2.9}$$

The majority of reinforcement learning algorithms is based on computing (or estimating) the value functions, which can then be used to control the behavior of the agent. We also

note a fundamental property of the value functions, which satisfy particular recursive relationships like the following *Bellman equation for* V^π:

$$\begin{aligned} V^\pi(s) &= E_\pi[R_t|s_t = s] \\ &= E_\pi[\sum_{k=0}^{\infty} \gamma^k r_{t+k+1}|s_t = s] \\ &= E_\pi[r_{t+1} + \gamma \sum_{k=0}^{\infty} \gamma^k r_{t+k+2}|s_t = s] \qquad (2.10) \\ &= \sum_{a\in A} \pi(s,a) \sum_{s'\in S} P(s,a,s') \Big[R(s,a) + \\ &\quad + \gamma E_\pi[\sum_{k=0}^{\infty} \gamma^k r_{t+k+2}|s_{t+1} = s']\Big] \qquad (2.11) \\ &= \sum_{a\in A} \pi(s,a) \sum_{s'\in S} P(s,a,s')[R(s,a) + \gamma V^\pi(s')] \qquad (2.12) \end{aligned}$$

Intuitively, Equation (2.12) decomposes the state-value function as the sum of the immediate reward collected from a state s to a successor state s', and the value of s' itself; by considering the transition model of the MDP and the policy being followed, we see that the Bellman equation simply averages the expected return over all the possible (s, a, r, s') transitions, by taking into account the probability that these transitions occur.

2.2.2 Optimal Value Functions

In general terms, *solving* a reinforcement learning task consists in finding a policy that yields a sufficiently high expected return. In the case of MDPs with discrete state and actions sets[2], it is possible to define the concept of *optimal policy* as the policy that maximizes the expected return collected by the agent in an episode.

We start by noticing that state-value functions define a partial ordering over policies as follows:

$$\pi \geq \pi' \iff V^\pi(s) \geq V^{\pi'}(s), \forall s \in S$$

From this, the *optimal policy* π^* of an MDP is a policy that is better or equal than all other policies in the policy space. It has also been proven that among all optimal policies for an MDP, there is always a deterministic one (see Section 2.2.3).

The state-value function associated to π^* is called the *optimal state-value function*, denoted V^* and defined as:

$$V^*(s) = \max_\pi V^\pi(s), \forall s \in S \qquad (2.13)$$

[2]We make this clarification for formality, but we do not expand the details further in this work. Refer to Sutton and Barto [41] for more details on the subject of continuous MDPs.

As we did when introducing the value functions, given an optimal policy for the MDP it is also possible to define the *optimal action-value function* denoted Q^*:

$$Q^*(s,a) = \max_\pi Q^\pi(s,a) \tag{2.14}$$
$$= E[r_{t+1} + \gamma V^*(s_{t+1})|s_t = s, a_t = a] \tag{2.15}$$

Notice that Equation (2.15) in this definition highlights the relation between Q^* and V^*.

Since V^* and Q^* are value functions of an MDP, they must satisfy the same type of recursive relations that we described in Equation (2.12), in this case called the *Bellman optimality equations*. The Bellman optimality equation for V^* expresses the fact that the value of a state associated to an optimal policy must be the expected return of the best action that the agent can take in that state:

$$V^*(s) = \max_a Q^*(s,a) \tag{2.16}$$
$$= \max_a E_{\pi^*}[R_t|s_t = s, a_t = a] \tag{2.17}$$
$$= \max_a E_{\pi^*}[\sum_{k=0}^{\infty} \gamma^k r_{t+k+1}|s_t = s, a_t = a] \tag{2.18}$$
$$= \max_a E_{\pi^*}[r_{t+1} + \gamma \sum_{k=0}^{\infty} \gamma^k r_{t+k+2}|s_t = s, a_t = a] \tag{2.19}$$
$$= \max_a E_{\pi^*}[r_{t+1} + \gamma V^*(s_{t+1})|s_t = s, a_t = a] \tag{2.20}$$
$$= \max_a \sum_{s' \in S} P(s,a,s')[R(s,a) + \gamma V^*(s')] \tag{2.21}$$

The Bellman optimality equation for Q^* is again obtained from the definition as:

$$Q^*(s,a) = E[r_{t+1} + \gamma \max_{a'} Q^*(s_{t+1}, a')||s_t = s, a_t = a] \tag{2.22}$$
$$= \sum_{s'} P(s,a,s')[R(s,a) + \gamma \max_{a'} Q^*(s', a')] \tag{2.23}$$

Notice that both Bellman optimality equations have a unique solution independent of the policy. If the dynamics of the environment (R and P) are fully known, it is possible to solve the system of equations associated to the value functions (i.e. one equation for each state in S) and get an exact value for V^* and Q^* in each state.

2.2.3 Value-based Optimization

One of the main algorithm classes for solving reinforcement learning problems is based on searching an optimal policy for the MDP by computing either of the optimal value functions, and then deriving a policy based on them. From V^* or Q^*, it is easy to determine an optimal, deterministic policy:

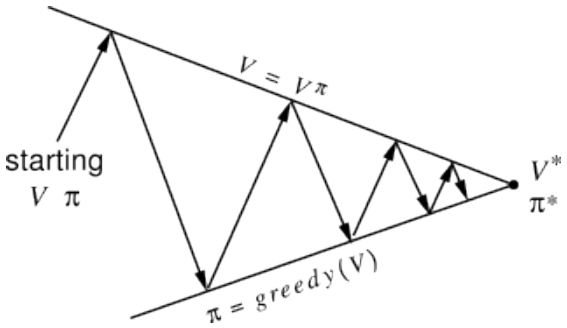

Figure 2.12: Classical representation of the policy iteration algorithm, which highlights the relation between policies and their associated value functions. Each pair of arrows starting from a policy and ending on a greedy policy based on the value function is a step of the algorithm.

- Given V^*, for each state $s \in S$ there will be an action (or actions) that maximizes the Bellman optimality equation (2.16). Any policy that assigns positive probability to only this action is an optimal policy. This approach therefore consists in performing a one-step forward search on the state space to determine the best action from the current state.

- Given Q^*, the optimal policy is the one that assigns positive probability to the action that maximizes $Q^*(s, a)$; this approach exploits the intrinsic property of the action-value function of representing the *quality* of actions, without performing the one-step search on the successor states.

In the following sections, we will describe some of the most important value-based approaches to RL, which will be useful in the following chapters of this thesis. We will not deal with equally popular methods like *policy gradient* or *actor-critic* approaches, even though they have been successfully applied in conjunction with DL to solve complex environments (see Chapter 3).

2.2.4 Dynamic Programming

The use of dynamic programming (DP) techniques to solve reinforcement learning problems is based on recursively applying some form of the Bellman equation, starting from an initial policy or value function until convergence to an optimal policy or value function. In this class of algorithms, we identify two main approaches: *policy iteration* and *value iteration*.

Policy Iteration

Policy iteration is based on the following theorem:

Theorem 1 (Policy improvement theorem) *Let π and π' be a pair of deterministic policies such that*

$$Q^{\pi}(s, \pi'(s)) \geq V^{\pi}(s), \forall s \in S$$

Then, $\pi' \geq \pi$, i.e.

$$V^{\pi'}(s) \geq V^{\pi}(s), \forall s \in S$$

This approach works by iteratively computing the value function associated to the current policy, and then improving that policy by making it act greedily with respect to the value function (as shown in Figure 2.12), such that:

$$\pi'(s) = \arg\max_{a \in A} Q^{\pi}(s, a) \tag{2.24}$$

For Theorem 1, the expected return of the policy is thus improved because:

$$Q^{\pi}(s, \pi'(s)) = \max_{a \in A} Q^{\pi}(s, a) \geq Q^{\pi}(s, \pi(s)) = V^{\pi}(s) \tag{2.25}$$

This continuous improvement is applied until Inequality (2.25) becomes an equality, i.e. until the improved policy satisfies the Bellman optimality equation (2.16). Since the algorithm gives no assurances on the number of updates required for convergence, some stopping conditions are usually introduced to end the process when the new value function does not change substantially after the update (*ε-convergence*) or a certain threshold number of iterations has been reached.

Value Iteration

Based on a similar idea, the *value iteration* approach starts from an arbitrary value function, and then applies a contraction operator which iterates over sequentially better value functions without actually computing the associated greedy policy. The contraction operator which ensures convergence is the *Bellman optimality backup*:

$$V_{k+1}(s) \leftarrow \max_{a} \sum_{s'} P(s, a, s')[R(s, a) + \gamma V(s')] \tag{2.26}$$

As with policy iteration, convergence is ensured without guarantees on the number of steps, and therefore it is usual to terminate the iteration according to some stopping condition.

2.2.5 Monte Carlo Methods

Dynamic programming approaches exploit the exact solution of a value function that can be computed starting from a policy, but in general this requires to have a perfect knowledge of the environment's dynamics and may also not be tractable on sufficiently complex MDPs.

Monte Carlo (MC) methods are a way of solving reinforcement learning problems by only using *experience*, i.e. a collection of *sample trajectories* from an actual interaction of an agent with the environment. This is often referred to as a *model-free* approach because, while the environment (or a simulation thereof) is still required to observe the sample trajectories, it is not necessary to have an exact knowledge of the transition model and reward function of the MDP.

Despite the differences with dynamic programming, this approach is still based on the same two-step process of policy iteration (evaluation and improvement). To estimate the value of a state $V^\pi(s)$ under a policy π with Monte Carlo methods, it is sufficient to consider a set of episodes collected under π: the value of the state s will be computed as the average of the returns collected following a *visit* of the agent to s, for all occurrences of s in the collection[3].

This same approach can be also used to estimate the action-value function, simply by considering the occurrence of state-action pairs in the collected experience rather than states only.

Finally, the policy is improved by computing its greedy variation (2.24) with respect to the estimated value functions and the process is iteratively repeated until convergence, with a new set of trajectories collected under each new policy.

2.2.6 Temporal Difference Learning

Temporal Difference (TD) learning is an approach to RL that uses concepts from both dynamic programming and Monte Carlo techniques. TD is a *model-free* approach that uses experience (like in MC) to update an estimate of the value function by using a previous estimate (like in DP). Like MC, TD estimation uses the rewards following a visit to a state to compute the value function, but with two core differences:

1. Instead of the average of all rewards following the visit, a single time step is considered (this is true for the simplest TD approach, but note that in general an arbitrary number of steps can be used; the more steps are considered, the more the estimate is similar to the MC estimate).

2. Estimates of the value function are updated by using in part an already computed estimate. For this reason, this approach is called a *bootstrapping* method (like DP). Specifically, the iterative update step for the value function is:

$$V(s_t) \leftarrow V(s_t) + \alpha[r_{t+1} + \gamma V(s_{t+1}) - V(s_t)] \tag{2.27}$$

In general, TD methods have several advantages over MC as they allow for an *on-line* (i.e. they don't require full episode trajectories to work), bootstrapped, *model-free*

[3]Note that a variation of this algorithm exists, which only considers the average returns following the *first* visit to a state in each episode.

estimate, which is more suitable for problems with long or even infinite time horizons. Moreover, TD is less susceptible to errors and to the effects of exploratory actions, and in general provides a more stable learning. It must be noted, however, that both TD and MC are guaranteed to converge given a sufficiently large amount of experience, and that there are problems for which either of the two can converge faster to the solution.

We will now present the two principal control algorithms in the TD family, one said to be *on-policy* (i.e. methods that attempt to evaluate and improve the same policy that they use to make decisions) and the other *off-policy* (i.e. methods with no relations between the estimated policy and the policy used to collect experience).

SARSA

As usual in *on-policy* approaches, *SARSA*[4] works by estimating the value $Q^\pi(s, a)$ for a current behavior policy π which is used to collect sample transitions from the environment. The policy is updated towards greediness with respect to the estimated action-value after each transition (s, a, r, s', a'), and the action-value is in turn updated step-wise with the following rule:

$$Q(s_t, a_t) \leftarrow Q(s_t, a_t) + \alpha[r_{t+1} + \gamma Q(s_{t+1}, a_{t+1}) - Q(s_t, a_t)] \tag{2.28}$$

The training procedure of SARSA can be summarized with Algorithm 1.

Convergence of the SARSA method is guaranteed by the dependence of π on the action-value function, as long as all state-action pairs are visited an infinite number of times and the policy converges in the limit to the greedy policy (e.g. a time-dependent ε-greedy policy with $\varepsilon = 1/t$).

Q-learning

Introduced by Watkins in 1992 [46], and considered by Sutton and Barto [41] as one of the most important breakthroughs in reinforcement learning, *Q-learning* is an *off-policy* temporal difference method that approximates the optimal action-value function independently of the policy being used to collect experiences. This simple, yet powerful idea guarantees convergence to the optimal value function as long as all state-action pairs are continuously visited (i.e. updated) during training.

The update rule for the TD step in Q-learning is the following:

$$Q(s_t, a_t) \leftarrow Q(s_t, a_t) + \alpha[r_{t+1} + \gamma \max_a Q(s_{t+1}, a) - Q(s_t, a_t)] \tag{2.29}$$

As we did for SARSA, a procedural description of the Q-learning algorithm is provided in Algorithm 2.

[4]Originally called *online Q-learning* by the creators; this alternative acronym was proposed by Richard Sutton and reported in a footnote of the original paper in reference to the *State, Action, Reward, next State, next Action* tuples which are used for prediction.

Algorithm 1 SARSA

Initialize $Q(s, a)$ arbitrarily
Initialize π as some function of Q (e.g. greedy)
repeat
  Initialize s
  Choose a from s using π
  repeat
    Take action a, observe r, s'
    Choose a' from s' using π
    Update $Q(s, a)$ using Rule (2.28)
    if π is time-variant **then**
      Update π towards greediness
    end if
    $s \leftarrow s'$; $a \leftarrow a'$
  until s is terminal or Q did not change
until training ended or Q did not change

Algorithm 2 Q-Learning

Initialize $Q(s, a)$ and π arbitrarily
repeat
  Initialize s
  repeat
    Choose a from s' using π
    Take action a, observe r, s'
    Update $Q(s, a)$ using Rule (2.29)
    $s \leftarrow s'$
  until s is terminal or Q did not change
until training ended or Q did not change

2.2.7 Fitted Q-Iteration

Having introduced a more classic set of traditional RL algorithms in the previous sections, we now present a more modern technique to solve MDPs with the use of supervised learning algorithms to estimate the value functions.

As we will see later in this thesis, the general idea of estimating the value functions with a supervised model is not an uncommon approach, and it has been often used in the literature to solve a wide range of environments with high-dimensional state-action spaces. This is especially useful in problems for which the closed form solutions of DP, or the guarantees of visiting all state-action pairs required for MC and TD, are not feasible.

Here, we choose the *Fitted Q-Iteration* (FQI) [11] algorithm as representative for this whole class, because it will be used in later sections of this thesis as a key component of the presented methodology. FQI is an *off-line*, *off-policy*, *model-free*, *value-based* reinforcement learning algorithm that computes an approximation of the optimal policy from a set of four-tuples (s, a, r, s') collected by an agent under a policy π. This approach is usually referred to as *batch mode* reinforcement learning, because the complete amount of learning experience is fixed and given a priori.

The core idea behind the algorithm is to produce a sequence of approximations of Q^π, where each approximation is associated to one step of the *value-iteration* algorithm seen in Section 2.2.4, and computed using the previous approximation as part of the target for the supervised learning problem. The process is described in Algorithm 3.

Algorithm 3 Fitted Q-Iteration

Given: a set F of four-tuples $(s \in S, a \in A, r \in \mathbb{R}, s' \in S)$ collected with some policy π; a regression algorithm;
$N \leftarrow 0$
Let $\hat{Q}_N$ be a function equal to 0 everywhere on $S \times A$
repeat
  $N \leftarrow N + 1$
  $TS \leftarrow ((x_i, y_i), i = 0, \ldots, |F|)$ such that $\forall (s_i, a_i, r_i, s'_i) \in F$:
    $x_i = (s_i, a_i)$
    $y_i = r_i + \gamma \max_{a \in A} \hat{Q}_{N-1}(s'_i, a)$
  Use the regression algorithm to induce $\hat{Q}_N(s, a)$ from TS
until stopping condition is met

Note that at the first iteration of the algorithm the action-value function is initialized as a null constant, and therefore the first approximation computed by the algorithm is that of the reward function. Subsequent iterations use the previously estimated function to compute the target of a new supervised learning problem, and therefore each step

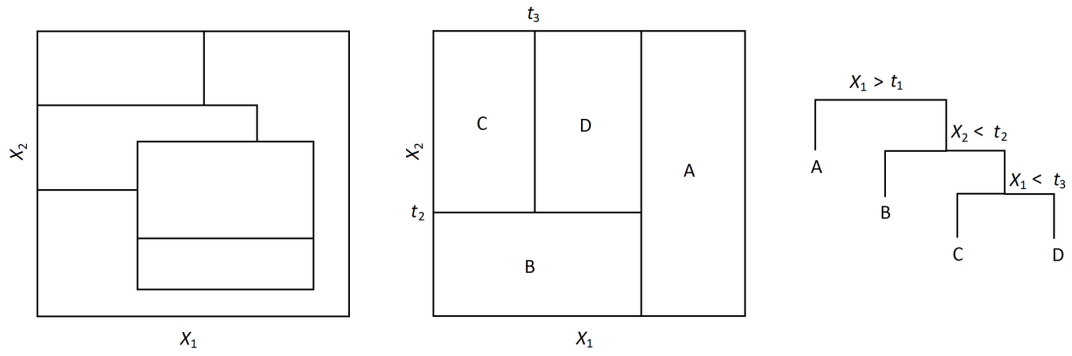

Figure 2.13: A 2D space partitioned with a random splitting algorithm (left) and recursive splitting (center); the recursively partitioned feature space can then be converted to a decision tree (right).

is independent from the previous one, except for the information of the environment stored in the computed approximation.

A more practical description on how to apply this algorithm to a real problem will be detailed in later sections of this thesis. For now, we limit this section to a more abstract definition of the algorithm and we do not expand further on the implementation details.

2.3 Additional Formalism

In this section we briefly introduce some additional algorithms and concepts that will be used in later chapters as secondary components of our approach.

2.3.1 Decision Trees

Decision trees are a non-parametric supervised learning method for classification and regression. A decision tree is a tree structure defined over a domain (*attributes*) and co-domain (*labels*), in which each internal node represents a boolean test on an attribute and each leaf node represents a label. Given a set of attributes for a data point, the tests are applied to the attributes starting from the root until a leaf is reached, and the corresponding label is output by the model.

To learn a decision tree, the input space is partitioned recursively by splitting a subset of the space according to a binary condition, in a greedy procedure called *Top-Down Induction of Decision Trees* (TDIDT) based on *recursive binary partitioning* (see Figure 2.13). This recursive procedure is iterated over the input space until all training samples belonging to a partition have the same label, or splitting the domain further would not add information to the model. At each step, the attribute which best splits

the training samples is selected for splitting, where the quality of the split is determined according to different criteria such as:

- *Gini impurity*, the probability of incorrectly labeling a random training sample, if it was randomly labeled according to the distribution of labels in the partition. Attributes with low Gini impurity are selected with a higher priority. The measure is defined for a set as:

$$I_G(S) = \sum_{i=1}^{K} p_i(1 - p_i) \tag{2.30}$$

  where S is a set of samples with labels $\{1, ..., K\}$ and p_i is the fraction of samples with label i in the set;

- *information gain*, the expected change in information entropy resulting form the split. To build a tree, the information gain of each possible split is computed and the most informative split is selected. The process is then repeated iteratively until the tree is complete. The measure is defined as the difference of entropy between a father node and a weighted sum of the children's entropy, where entropy is:

$$H(S) = -\sum_{i=1}^{K} p_i \log p_i \tag{2.31}$$

  and the information gain is formalized as:

$$I_I(S, a) = H(S) - H(S|a) \tag{2.32}$$

  for a set S and a split a;

- *variance reduction*, typically used in regression trees (with a continuous co-domain), it quantifies the total reduction of the variance in the target after the split. Attributes with higher variance reduction are selected for splitting with higher priority. The metric is computed as:

$$\begin{aligned} I_V(S) = & \frac{1}{|S^{All}|^2} \sum_{i \in S^{All}} \sum_{j \in S^{All}} \frac{1}{2}(x_i - x_j)^2 + \\ & - \frac{1}{|S^T|^2} \sum_{i \in S^T} \sum_{j \in S^T} \frac{1}{2}(x_i - x_j)^2 + \\ & - \frac{1}{|S^F|^2} \sum_{i \in S^F} \sum_{j \in S^F} \frac{1}{2}(x_i - x_j)^2 \end{aligned} \tag{2.33}$$

  where S^{All} is the set of all sample indices in the set S, S^T is the partition of indices for which the attribute test is true, and S^F is the partition of indices for which the attribute test is false.

2.3.2 Extremely Randomized Trees

Extremely Randomized Trees (Extra-Trees) [14] is a tree-based ensemble method for supervised learning that consists in strongly randomizing both attribute and cut-point choice while splitting a decision tree node. The Extra-Trees algorithm builds an ensemble of M unpruned decision trees according to the classical top-down procedure, but differently from other tree induction methods it splits nodes by choosing cut-points fully at random. Extra-Trees can be applied to both classification and regression by building an ensemble of trees for either task.

The procedure to randomly split a node when building the ensemble is summarized in Algorithm 4.

The procedure has three main parameters:

- M, the number of decision trees to build for the ensemble;
- K, the number of attributes randomly selected at each node;
- n_{min}, the minimum sample size for splitting a node.

In the prediction phase, the output of each tree in the ensemble is aggregated to compute the final prediction, with a majority voting in classification problems and an arithmetic average in regression problems.

Algorithm 4 Extra-Trees node splitting

Split_node(S):
  Given: the local learning subset S corresponding to the node we want to split
  if Stop_split(S) is True **then**
    Return nothing
  else
    Select K attributes $\{a_1, ..., a_k\}$ among all non constant candidate attributes in S
    Draw K splits $\{S_1, ..., S_k\}$ where $S_i =$**Pick_random_split**(S, a_i)
    Return a split S_* such that $Score(S_*, S) = \max_i Score(S_i, S)$
  end if

Pick_random_split(S, a):
  Given: a subset S and an attribute a
  Let a^S_{max} and a^S_{min} denote the maximal and minimal value of a in S
  Draw a random cut-point a_c uniformly in $[a^S_{min}, a^S_{max}]$
  Return the split $[a < a_c]$

Stop_split(S):
  Given: a subset S
  if $|S| < n_{min}$ **then**
    Return True
  end if
  if All attributes are constant in S **then**
    Return True
  end if
  if The output is constant in S **then**
    Return True
  end if
  Return False

Chapter 3

State of the Art

The integration of RL and neural networks has a long history. Early RL literature [37, 43, 4] presents *connectionist* approaches in conjunction with a variety of RL algorithms, mostly using dense ANNs as approximators for the value functions from low-dimensional (or engineered) state spaces. However, the recent and exciting achievements of DL have caused a sort of RL renaissance, with DRL algorithms outperforming classic RL techniques on environments that were previously considered intractable. Much like the game of Chess was believed out of the reach of machines until IBM's Deep Blue computer [7] won against world champion Garry Kasparov in 1997, DRL has paved the way to solve a wide spectrum of complex tasks that have always been a stronghold of humanity.

In this chapter we present the most important and recent results of DRL research, as well as some work related to the algorithm proposed in this thesis.

3.1 Value-based Deep Reinforcement Learning

In 2013, Mnih et al. [32] introduced the *deep Q-learning* (DQN) algorithm, which basically ignited the field of DRL. The important contributions of DQN consisted in providing an end-to-end framework to train an agent on the *Atari* environments (Figure 3.2) starting from the pixel-level representation of the states, with a deep CNN (called *deep Q-network*[1]; see Figure 3.1) used to estimate the Q function and apply greedy control. The authors were able to reuse the same architecture to solve many different games without the need for *hyperparameter tuning*, which proved the effectiveness of the method.

The key idea of DQN is to embed the update step of Q-learning into the loss used

[1] Hence the acronym *DQN*.

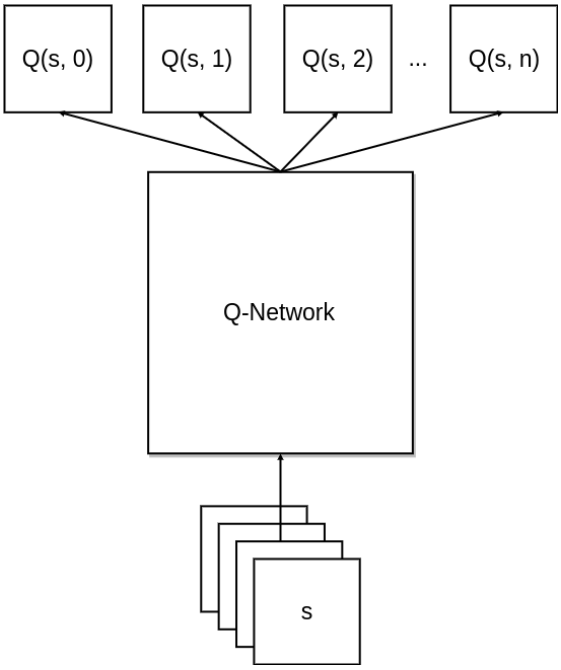

Figure 3.1: Structure of the Deep Q-Network by Mnih et al..

for SGD to train the deep CNN, resulting in the following gradient update:

$$\frac{\partial L}{\partial W_i^{old}} = E[(r + \gamma \max_{a'} Q(s', a'; \theta') - Q(s, a)) \frac{\partial Q(s, a; \theta)}{\partial W_i^{old}}] \tag{3.1}$$

where θ, θ' indicate two different sets of parameters for the CNN, which are respectively called the *online network* (θ) to select the action for the collection of samples, and the *target network* (θ') to produce the update targets. The online network is continuously updated during training, whereas the target network is kept fixed for longer time intervals in order to stabilize the online estimate. Moreover, a sampling procedure called *experience replay* [29] is used to stabilize training. This consists in keeping a variable training set of transitions collected with increasingly better policies (starting from a fully random ε-greedy policy and decreasing ε as the Q estimate improves), from which training samples are randomly selected. The full training procedure of DQN is reported in Algorithm 5.

From this work (which we could call introductory), many improvements have been proposed in the literature. Van Hasselt et al. (2016) proposed *Double DQN* (DDQN) [20] to solve an over-estimation issue typical of Q-learning, due to the use of the maximum action value as an approximation for the maximum expected action value (see Equation (2.29)). This general issue was addressed by Van Hasselt (2010) with *Double Q-learning* [19], a learning algorithm that keeps two separate estimates of the action-value function

Algorithm 5 Deep Q-Learning with Experience Replay

Initialize replay memory $\mathcal{D}$ to capacity N
Initialize action-value function Q with two random sets of weights θ, θ'
for *episode* $= 1, M$ **do**
  for $t = 1, T$ **do**
    Select a random action a_t with probability ε
    Otherwise, select $a_t = \arg\max_a Q(s_t, a; \theta)$
    Execute action a_t, collect reward r_{t+1} and observe next state s_{t+1}
    Store the transition $(s_t, a_t, r_{t+1}, s_{t+1})$ in $\mathcal{D}$
    Sample mini-batch of transitions $(s_j, a_j, r_{j+1}, s_{j+1})$ from $\mathcal{D}$
    Set $y_j = \begin{cases} r_{j+1}, & \text{if } s_{j+1} \text{ is terminal} \\ r_{j+1} + \gamma \max_{a'} Q(s_{j+1}, a'; \theta'), & \text{otherwise} \end{cases}$
    Perform a gradient descent step using targets y_j with respect to the online parameters θ
    Every C steps, set $\theta' \leftarrow \theta$
  end for
end for

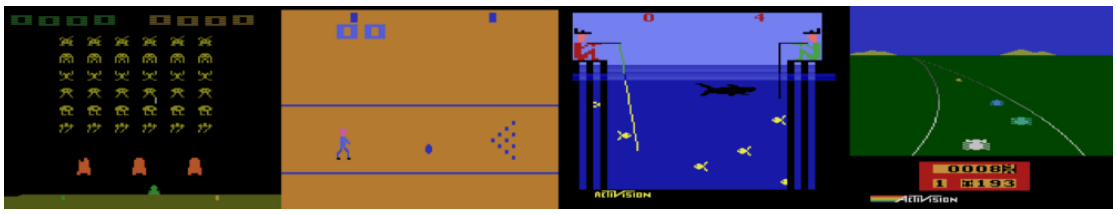

Figure 3.2: Some of the games available in the Atari environments.

Q^A and Q^B, and uses one to update the other as follows:

$$Q^A(s,a) \leftarrow Q^A(s,a) + \alpha[r + \gamma Q^B(s', \arg\max_a Q^A(s',a)) - Q^A(s,a)] \tag{3.2}$$

and vice-versa for Q^B. DDQN uses a similar approach to limit over-estimation in DQN by evaluating the greedy policy according to the online network, but using the target network to estimate its value. This is achieved with a small change in the computation of the update targets:

$$y_j = \begin{cases} r_{j+1}, & \text{if } s_{j+1} \text{ is terminal} \\ r_{j+1} + \gamma Q(s_{j+1}, \arg\max_a Q(s_{j+1}, a; \theta); \theta'), & \text{otherwise} \end{cases} \tag{3.3}$$

DDQN performed better (higher median and mean score) on the 49 Atari games used as benchmark by Mnih et al. (2015), equaling or even surpassing humans on several games.

Schaul et al. (2016) [38] developed the concept of *prioritized experience replay*, which replaced DQN's uniform sampling strategy from the replay memory with a sampling strategy weighted by the *TD errors* committed by the network. This improved the performance of both DQN and DDQN.

Wang et al. (2016) introduced a slightly different end-to-end *dueling architecture* [45], composed of two different deep estimators: one for the state-value function V and one for the *advantage function* $A : S \times A \to \mathbb{R}$ defined as:

$$A^\pi(s,a) = Q^\pi(s,a) - V^\pi(s) \tag{3.4}$$

In this approach, the two networks share the same convolutional layers but use two separate dense layers. The two streams are then combined to estimate the optimal action-value function as[2]:

$$Q^\pi(s,a) = V^\pi(s) + (A^\pi(s,a) - \max_{a'} A^\pi(s,a')) \tag{3.5}$$

Several other extensions of the DQN algorithm have been proposed in recent years. Among these, we cite Osband et al. (2016) [35] who proposed a better exploration strategy based on Thompson sampling, to select an exploration policy based on the probability that it is the optimal policy; He et al. (2017) [21] added a constrained optimization approach called *optimality tightening* to propagate the reward faster during updates and improve accuracy and convergence; Anschel et al. (2017) [2] improved the variance and instability of DQN by averaging previous Q estimates; Munos et al. (2016) [33] and Harutyunyan et al. (2016) [17] proposed to incorporate on-policy samples to the Q-learning target and seamlessly switch between off-policy and on-policy samples, which again resulted in faster reward propagation and convergence.

3.2 Other Approaches

In this section we present some approaches proposed in DRL literature as alternative to value-based DRL, characterized by unconventional architectures (e.g. *memory* modules in Section 3.2.1) or designed for a specific environment (e.g. the game of *Go* in Section 3.2.2).

3.2.1 Memory Architectures

Graves et al. (2016) [16] proposed *Differentiable Neural Computer* (DNC), an architecture in which an ANN has access to an external memory structure, and learns to read

[2] In the original paper, the authors explicitly indicate the dependence of the estimates on different parameters (e.g. $V^\pi(s,a;\phi,\alpha)$ where ϕ is the set of parameters of the convolutional layers and α of the dense layers). For simplicity in the notation, here we report the estimates computed by the network with the same notation as the estimated functions (i.e. the network which approximates V^π is indicated as V^π, and so on...).

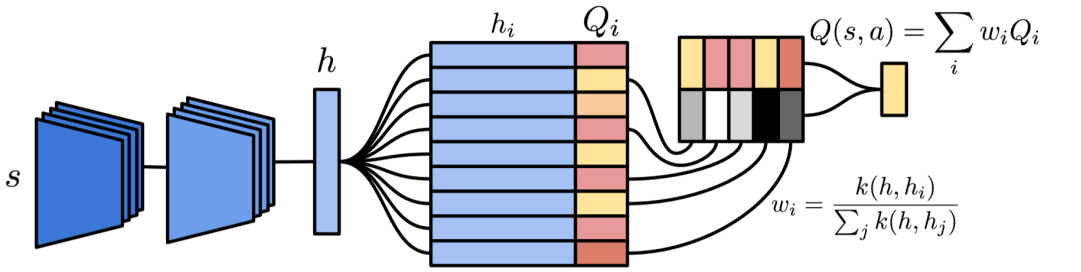

Figure 3.3: Architecture of NEC (image taken from [36]).

and write data by gradient descent in a goal-oriented manner. This approach outperformed normal ANNs and DNC's precursor *Neural Turing Machine* [15] on a variety of query-answering and natural language processing tasks, and was used to solve a simple *moving block* puzzle with a form of reinforcement learning in which a sequence of instructions describing a goal is coupled to a reward function that evaluates whether the goal is satisfied (a set-up that resembles an animal training protocol with a symbolic task cue).

Pritzel et al. (2017) [36] extended the concept of differentiable memory to DQN with *Neural Episodic Control* (NEC). In this approach, the DRL agent consists of three components: a CNN that processes pixel images, a set of memory modules (one per action), and a dense ANN that converts read-outs from the action memories into action-values. The memory modules, called *differentiable neural dictionaries* (DNDs), are memory structures that resemble the dictionary data type found in computer programs. DNDs are used in NEC to associate the state embeddings computed by the CNN to a corresponding Q estimate, for each visited state: a read-out for a key consists in a weighted sum of the values in the DND, with weights given by normalized kernels between the lookup key and the corresponding key in memory (see Figure 3.3). DNDs are populated automatically by the algorithm without learning what to write, which greatly speeds up the training time with respect to DNC.

NEC outperformed every previous DRL approach on the Atari games, by achieving better results using less training samples.

3.2.2 AlphaGo

Traditional board games like chess, checkers, Othello and Go are classical test benches for artificial intelligence. Since the set of rules that characterizes this type of games is fairly simple to represent in a program, the difficulty in solving these environments stems from the dimensionality of the state space. Among the cited games, Go was one of the last board games in which an algorithm had never beaten top human players, because its

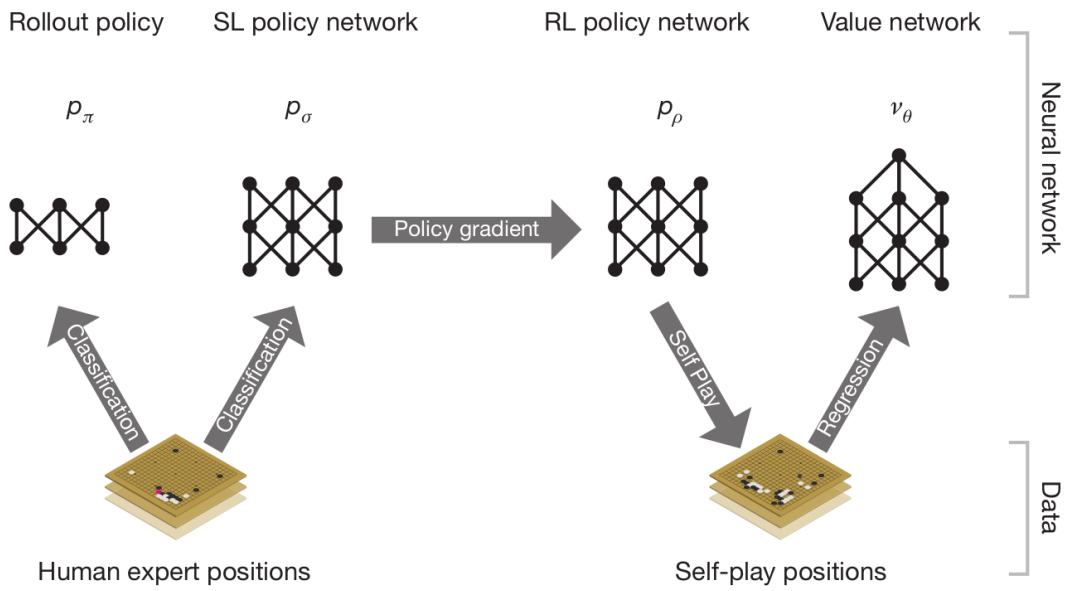

Figure 3.4: Neural network training pipeline of AlphaGo (image taken from [39]).

characteristic 19×19 board, which allows for approximately 250^{150} sequences of moves[3], was too complex for exhaustive search methods.

Silver et al. (2016) [39] introduced *AlphaGo*, a computer program based on DRL which won 5 games to 0 against the European Go champion in October 2015; soon after that, AlphaGo defeated 18-time world champion Lee Sedol 4 games to 1 in March 2016, and world champion Ke Jie 3 to 0 in May 2017. After these results, Google DeepMind (the company behind AlphaGo) decided to retire the program from official competitions and released a dataset containing 50 self-play games [18]. AlphaGo is a complex architecture that combines deep CNNs, reinforcement learning, and Monte Carlo Tree Search (MCTS) [6, 13]. The process is divided in two phases: a neural network training pipeline and MCTS. In the training pipeline, four different networks are trained: a *supervised learning* (SL) policy network trained to predict human moves; a *fast* policy network to rapidly sample actions during MC rollouts; a *reinforcement learning* policy network that improves the SL network by optimizing the final outcome of games of self-play; a *value* network that predicts the winner of games (see Figure 3.4). Finally, the policy and value networks are combined in an MCTS algorithm that selects actions with a lookahead search, by building a partial search tree using the estimates computed with each network.

[3]Number of legal moves per position elevated to the length of the game.

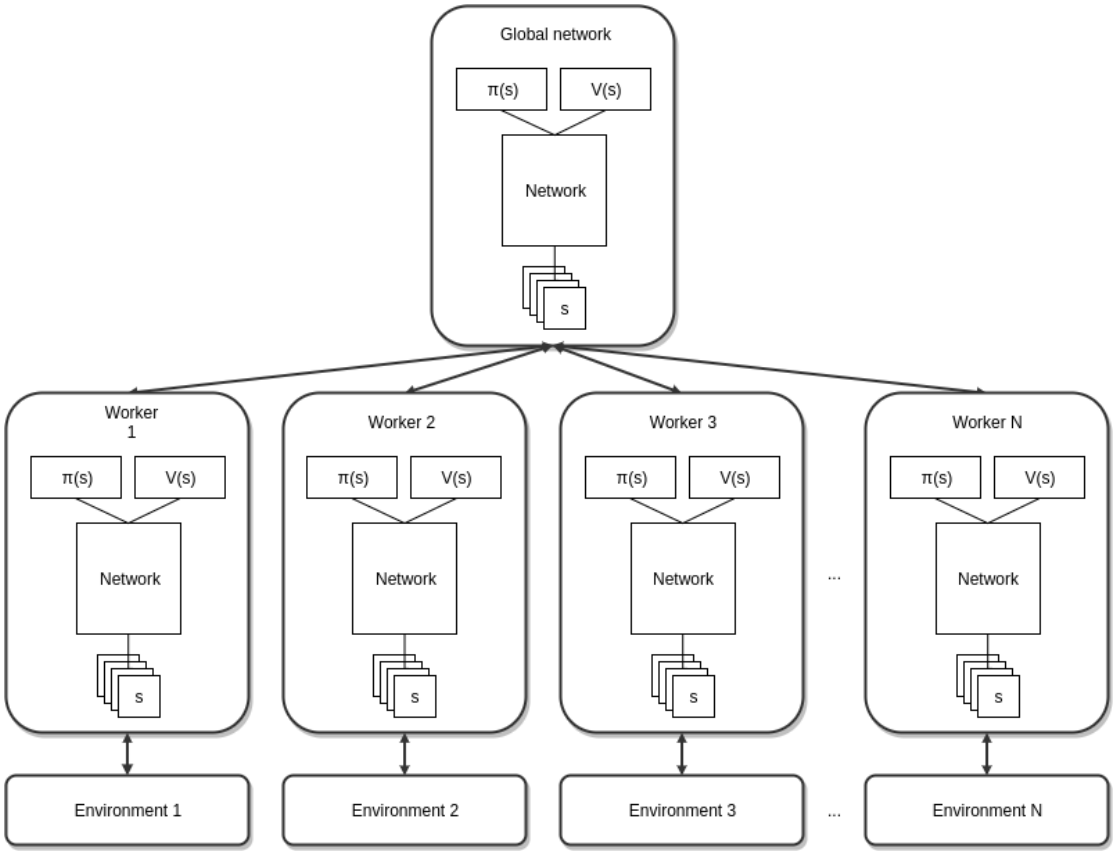

Figure 3.5: The asynchronous architecture of A3C.

3.2.3 Asynchronous Advantage Actor-Critic

Actor-critic algorithms [41] are RL methods that have a separate memory structure to explicitly represent the policy independent of the value function. The policy structure is known as the actor, because it is used to select actions, and the estimated value function is known as the critic, because it criticizes the actions made by the actor. Learning is always on-policy, as the critic must learn about and critique whatever policy is currently being followed by the actor. The critique usually takes the form of a TD error which is used to drive learning in both the actor and the critic, evaluated as:

$$\delta_t = r_{t+1} + \gamma V(s_{t+1}) - V(s_t) \tag{3.6}$$

Mnih et al. (2016) [31] presented a deep variation of the actor-critic algorithm, called *Asynchronous Advantage Actor-Critic* (A3C). In this approach, different instances of actor-critic pairs are run in parallel (Figure 3.5) to obtain a lower-variance estimate of the value function, without the need of a replay memory to stabilize training. Each *worker* consists in a deep CNN with a unique convolutional section and two separate dense

networks on top, one for the value function and one for the policy. This asynchronous methodology was applied to other classical RL algorithms in the same paper; we only report the actor-critic variant as it was the best performing, with notably shorter training times than DQN and its variations, but a similar cumulative reward on the Atari games.

3.3 Related Work

Lange and Riedmiller (2010) [27] proposed the *Deep Fitted Q-iteration* (DFQ) algorithm, a batch RL method that used deep dense autoencoders to extract a state representation from pixel images. In this algorithm, a training set of (s, a, r, s') transitions is collected with a random exploration strategy, where s, s' are pixel images of two consecutive states. The samples are then used to train a dense autoencoder with two neurons in the innermost layer, which in turn is used to encode all states in the training set. This encoded dataset is then passed as input to FQI, which produces an estimate for the Q function using a kernel based approximator. A new policy is then computed from the estimated Q and the encoder, and the process is repeated starting with the new policy until the obtained Q is considered satisfactory. The authors applied DFQ to a simple *Gridworld* environment with fixed size and goal state, and were able to outperform other image-based feature extraction methods (like *Principal Components Analysis* [47]) with a good sample efficiency.

Chapter 4

Deep Feature Extraction for Sample-Efficient Reinforcement Learning

As central contribution of this thesis, we propose a DRL algorithm that combines the feature extraction capabilities of unsupervised deep CNNs with the fast and powerful batch RL approach of FQI. Given a control problem with high-dimensional states and a mono-dimensional discrete action space, we use a deep convolutional autoencoder to map the original state space to a compressed *feature space* that accounts for information on the states and the nominal dynamics of the environment (i.e. those changes not directly influenced by the agent). We reduce the representation further by applying the *Recursive Feature Selection* (RFS) algorithm to the extracted state features, and this minimal state space is then used to run the FQI algorithm. We repeat this procedure iteratively in a *semi-batch* approach to bootstrap the algorithm, starting from a fully random exploration of the environment.

In this chapter we give a formal description of the method and its core components, whereas technical details of implementation will be discussed in the next chapter.

4.1 Motivation

The state-of-the-art DRL methods listed in the previous chapter are able to outperform classic RL algorithms in a wide variety of problems, and in some cases are the only possible way of dealing with high-dimensional control settings like the Atari games. However, the approaches cited above tend to be grossly *sample-inefficient*, requiring tens of millions of samples collected online to reach optimal performance. Several publications successfully deal with this aspect, but nonetheless leave room for improvement (lower-

ing at most by one order of magnitude the number of samples required). The method introduced by Lange and Riedmiller (2010) [27] is similar to ours, but their dense architecture predates the more modern convolutional approaches in image processing and is less suited than our AE for complex tasks.

The method that we propose tries to improve both aspects of information content of the compressed feature space and sample efficiency. We extract general features from the environments in an unsupervised fashion, which forgoes the task-oriented representation of the current state-of-the-art methods in favor of a description that relates more closely to the original information content of the states; because of the generality of this description, the compressed state space can be used with a variety of RL algorithms in their default setting (like we show with FQI), without having to adapt the deep architecture to solve the problem end-to-end like in deep Q-learning. Moreover, since deep features can be difficult to interpret in an abstract way, and in general there is no assurance against redundancy in the representation, we use a feature selection technique on the extracted space in order to really minimize the description while retaining all information required for control. This additional step does not have a substantial impact on the learning phase, nor on the learned policies (since we do not extract features aimed at controlling, there is no direct correlation between features and performance, in general), but by providing an essential representation of the states it allows the feature extraction method to be stripped of all the useless parameters, resulting in reduced computational requirements during the control phase (an important aspect in some high-frequency sequential decision making problems). Finally, our sample-efficient methodology allows our agent to learn non-trivial policies using up to two orders of magnitude less samples than the state-of-the-art approaches, which may be important in those environments where online sample collection is difficult or expensive.

4.2 Algorithm Description

The general structure of this algorithm is typical of DRL settings: we use a deep ANN to extract a representation of an environment, and then use that representation to control an agent with standard RL algorithms. We also add an additional step after the deep feature extraction to further reduce the representation down to the essential bits of information required to solve the problem, by using the *Recursive Feature Selection* (RFS) [8] algorithm.

We focus exclusively on environments with a discrete and mono-dimensional action space $A = \{0, 1, ..., a\}$, where actions are assigned a unique integer identifier starting from 0 with no particular order. We also assume to be operating in a three dimensional state space ($channels \times height \times width$) for consistency with the experimental setting on which we tested the algorithm (with pixel-level state spaces), although in general the algorithm requires no such assumption and could be easily adapted to higher or lower

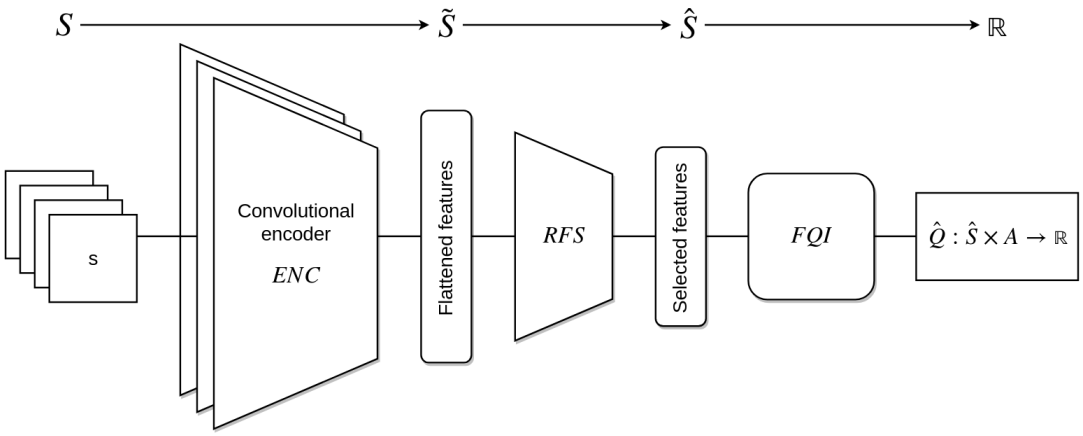

Figure 4.1: Composition of the three main modules of the algorithm to produce the end-to-end function $Q : S \times A \to \mathbb{R}$. Pixel-level states are transformed by the encoder into the 1D feature space $\tilde{S}$, which in turn is filtered by RFS into space $\hat{S}$. The final representation is used to train FQI, which outputs an action-value function $\hat{Q}$ on $\hat{S} \times A$. The same preprocessing pipeline is then required to use $\hat{Q}$, and the full composition of the three modules effectively consists in an action-value function on the original state-action space $S \times A$.

dimensional settings.

The algorithm uses a modular architecture with three different components that are combined after training to produce an approximator of the action-value function. The main components of the algorithm are:

1. a deep convolutional autoencoder that we use to extract a representation of the environment; the purpose of the AE is to map the original, pixel-level state space S of the environment into a strongly compressed feature space $\tilde{S}$, that contains information on both the states and part of the transition model of the environment;

2. the Recursive Feature Selection technique to further reduce the state representation $\tilde{S}$ and keep only the truly informative features extracted by the AE, effectively mapping the extracted feature space to a subspace $\hat{S}$.

3. the Fitted Q-Iteration learning algorithm to produce an estimator for the action-value function, with $\hat{S}$ as domain.

The full procedure consists in alternating a training step and an evaluation step, until the desired performance is reached.

A training step of the algorithm takes as input a training set $\mathcal{TS}$ of four-tuples $(s \in S, a \in A, r \in \mathbb{R}, s' \in S)$ to produce an approximation of the action-value function, and consists in sequentially training the three components from scratch to obtain the following transformations, respectively:

- $ENC : S \to \tilde{S}$, from the pixel representation to a compressed feature space;
- $RFS : \tilde{S} \to \hat{S}$, from the compressed feature space to a minimal subspace with the most informative features for control purposes;
- $\hat{Q} : \hat{S} \times A \to \mathbb{R}$, an approximation of the optimal action-value function on $\hat{S}$.

After training, we simply combine the three functions (see Figure 4.1) to obtain the full action-value function $Q : S \times A \to \mathbb{R}$ as follows:

$$Q(s, a) = \hat{Q}(RFS(ENC(s)), a) \tag{4.1}$$

To collect the training set $\mathcal{TS}$, we define a greedy policy π based on the current approximation of Q as:

$$\pi(s) = \arg\max_{a} Q(s, a) \tag{4.2}$$

and we use an ε-greedy policy π_ε based on π (cf. Section 2.2.1) to collect $\mathcal{TS}$. We initialize the ε-greedy policy as fully random (which means that we do not need an approximation of Q for the first step), and we decrease ε after each step down to a fixed minimum positive value ε_{min}. This results in a sufficiently high exploration at the beginning of the procedure, but increasingly exploits the learned knowledge to improve the quality of the collected samples after each training step, as the agent learns to reach states with a higher value. The lower positive bound on ε is kept to minimize overfitting and allow the agent to explore potentially better states even in the later steps of the algorithm. A similar approach, called *ε-annealing*, was used by Mnih et al. (2015) [32] for the online updates in DQN. Each training step is followed by an evaluation phase to determine the quality of the learned policy and eventually stop the procedure when the performance is deemed satisfactory. A general description of the process is reported in Algorithm 6, and details on the training phases and evaluation step are given in the following sections.

Note that in general the *semi-batch* approach, which starts from a training set collected under a fully random policy and sequentially collects new datasets as performance improves, is not strictly necessary. It is also possible to run a single training step in pure batch mode, using a dataset collected under an expert policy (albeit with some degree of exploration required by FQI) to produce an approximation of the optimal Q function in one step. This allows to exploit the sample efficiency of the algorithm in situations where, for instance, collecting expert samples is difficult.

4.3 Extraction of State Features

The AE used in our approach consists of two main components, namely an *encoder* and a *decoder* (cf. Section 2.1.4). To the end of explicitly representing the encoding purpose

Algorithm 6 Fitted Q-Iteration with Deep State Features

Given:

$\varepsilon_{min} \in (0, 1)$;

$\varphi : [\varepsilon_{min}, 1] \to [\varepsilon_{min}, 1)$ s.t. $\varphi(x) < x, \forall x \in (\varepsilon_{min}, 1]$ and $\varphi(\varepsilon_{min}) = \varepsilon_{min}$

Initialize the encoder $ENC : S \to \tilde{S}$ arbitrarily

Initialize the decoder $DEC : \tilde{S} \to S$ arbitrarily

Initialize Q arbitrarily

Define $\pi(s) = \arg\max_a Q(s, a)$

Initialize an ε-greedy policy π_ε based on π with $\varepsilon = 1$

repeat

Collect a set $\mathcal{TS}$ of four-tuples $(s \in S, a \in A, r \in \mathbb{R}, s' \in S)$ using π_ε

Train the composition $DEC \circ ENC : S \to S$ using the state elements $(s \in S)$ of $\mathcal{TS}$ as input and target

Build a set $\mathcal{TS}_{ENC}$ of four-tuples $(\tilde{s} \in \tilde{S}, a \in A, r \in \mathbb{R}, \tilde{s}' \in \tilde{S})$ by applying the encoder to the first and last elements of each four-tuple in $\mathcal{TS}$ s.t. $\tilde{s} = ENC(s)$

Call the RFS feature selection algorithm on $\mathcal{TS}_{ENC}$ to obtain a space reduction $RFS : \tilde{S} \to \hat{S}$

Build a set $\mathcal{TS}_{RFS}$ of four-tuples $(\hat{s} \in \hat{S}, a \in A, r \in \mathbb{R}, \hat{s}' \in \hat{S})$ by applying RFS to the first and last elements of each four-tuple in $\mathcal{TS}_{ENC}$ s.t. $\hat{s} = RFS(\tilde{s})$

Call FQI on $\mathcal{TS}_{RFS}$ to produce $\hat{Q} : \hat{S} \times A \to \mathbb{R}$

Combine $\hat{Q}$, RFS and ENC to produce $Q : S \times A \to \mathbb{R}$:

$$Q(s, a) = \hat{Q}(RFS(ENC(s)), a)$$

Set $\varepsilon \leftarrow \varphi(\varepsilon)$

Evaluate π

until stopping condition on evaluation performance is met

Return Q

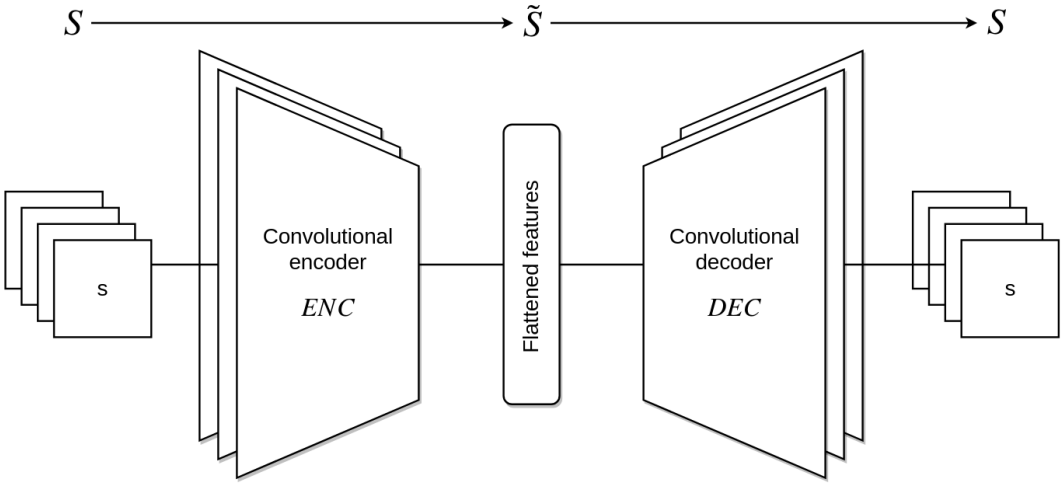

Figure 4.2: Schematic view of the AE.

of the AE, we keep a separate notation of the two modules; we therefore refer to two different CNNs, namely $ENC : S \to \tilde{S}$ to map the original state space to the compressed representation $\tilde{S}$, and $DEC : \tilde{S} \to S$ to perform the inverse transformation. The full AE is the composition of the two networks $AE : DEC \circ ENC : S \to S$ (Figure 4.2). Note that the composition is differentiable end-to-end, and basically consists in *plugging* the last layer of the encoder as input to the decoder. Both components are convolutional neural networks specifically structured to reduce the representation down to an arbitrary number of features in the new space. We train the AE to reconstruct its input in an unsupervised fashion, using a dataset $\mathcal{TS}$ of four-tuples $(s \in S, a \in A, r \in \mathbb{R}, s' \in S)$ collected with the ε-greedy policy and taking the first element $(s \in S)$ of each sample as input and target. The output of this phase is the trained encoder $ENC : S \to \tilde{S}$, which takes as input the three-dimensional states of the environment and produces a one-dimensional feature vector representing a high-level abstraction of the state space. We refer to $\tilde{S}$ as a representation of both the state and the nominal environment dynamics because we allow for the original state space S to contain both such types of information, accounting for changes in the environment that are not directly (or even indirectly) caused by the user. An example of this is the *MsPacman* environment in the Atari suite, implementation of the popular arcade game, in which the *ghosts* are able to move autonomously, not necessarily influenced by the player; in such a setting, the environment presents non-trivial nominal dynamics that must be taken into account in the extracted representation (Figure 4.3). Details on how we accomplish this are provided in the following chapter, when dealing with the specific implementation of our experimental setting.

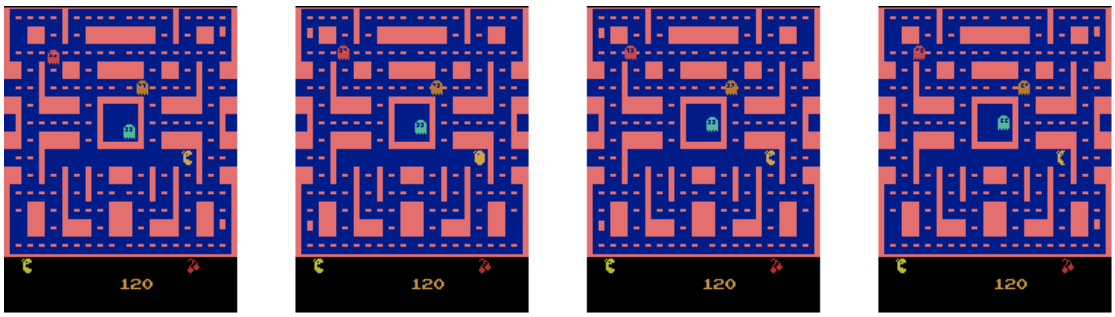

Figure 4.3: Example of non-trivial nominal dynamics in the MsPacman *environment, with the ghosts moving autonomously across the four consecutive observations.*

4.4 Recursive Feature Selection

The *Recursive Feature Selection* (RFS) [8] algorithm is a dimensionality reduction technique for control problems proposed by Castelletti et al. (2011). The algorithm identifies which state and action features (i.e. elements of the state and action vector spaces) are most relevant for control purposes, reducing the dimensionality of both spaces by removing the less important features. The core of the algorithm consists in recursively selecting the features that best explain the dynamics (i.e. the transition model) of the features already selected, starting from the subset of features needed to explain the reward function, using the *Iterative Feature Selection* (IFS) [12] algorithm to recursively build a dependency tree of features.

Algorithm 7 Recursive Feature Selection (RFS)

Given: a dataset $\mathcal{D} = \langle s \in S, a \in A, s' \in S \rangle$; a target feature F_0^i from the set of features of $S \cup A$; a set $\mathcal{F}_{sel}^i$ of previously selected features
$\mathcal{F}_{F_0}^i \leftarrow IFS(\mathcal{D}, F_0^i)$
$\mathcal{F}_{new}^i \leftarrow \mathcal{F}_{F_0}^i \setminus \mathcal{F}_{sel}^i$
for all $F_j^{i+1} \in \mathcal{F}_{new}^i$ **do**
  $\mathcal{F}_{F_0}^i \leftarrow \mathcal{F}_{F_0}^i \cup RFS(\mathcal{D}, F_j^{i+1}, \mathcal{F}_{sel}^i \cup \mathcal{F}_{F_0}^i)$
end for
return $\mathcal{F}_{F_0}^i$

The main procedure (summarized in Algorithm 7) takes as input a dataset $\mathcal{D}$ of observed transitions from an environment, the values of a target feature F_0^i in $\mathcal{D}$, and a set $\mathcal{F}_{sel}^i$ of previously selected features. The dataset and target feature are given as input to IFS, which returns a subset of features $\mathcal{F}_{F_0}^i$ that best explain the dynamics of F_0^i. RFS is then recursively called on each feature in the set $\mathcal{F}_{new}^i = \mathcal{F}_{F_0}^i \setminus \mathcal{F}_{sel}^i$ of new features selected by IFS. At the first step, the algorithm is usually run to identify the

most important features to explain the reward R by setting $F_0^0 = R$ and $\mathcal{F}_{sel}^0 = \emptyset$, so that the final output of the procedure will be a set of features that describe the dynamics of the reward and of the environment itself (a simple example of RFS is given in Figure 4.4).

The IFS procedure called at each step of RFS is a feature selection technique based on a *feature ranking* algorithm, but in general can be replaced by any feature selection method that is able to account for nonlinear dependencies and redundancy between features (as real-world control problems are usually characterized by nonlinear dynamics models with multiple coupled features). Here we use IFS for coherence with the paper by Castelletti et al., and because it is a computationally efficient feature selection algorithm that works well with our semi-batch approach. IFS takes as input a dataset $\mathcal{D}$ of observed (s, a, r, s') transitions from the environment and the values of a target feature F_0 in $\mathcal{D}$. The algorithm starts by globally ranking the features of the state space according to a statistical level of significance provided by a feature ranking method FR, which takes as input the dataset and the target feature; the most significant feature according to the ranking, F^*, is added to the set of selected features $\mathcal{F}_{sel}$. A supervised model $\hat{f}$ is then trained to approximate the target feature F_0, taking $\mathcal{F}_{sel}$ as input. The algorithm then proceeds by repeating the ranking process using as new target feature for FR the residual feature $\hat{F}_0 = F_0 - \hat{f}(\mathcal{F}_{sel})$ (the difference between the target value and the approximation computed by $\hat{f}$ for each sample in $\mathcal{D}$). The procedure continues to perform these operations until either the best variable in the feature ranking is already in $\mathcal{F}_{sel}$, or the accuracy of the model built upon $\mathcal{F}_{sel}$ does not improve. The accuracy of the model is computed with the coefficient of determination R^2 between the values of the target feature F_0 and the values $F_{pred} = \hat{f}(\mathcal{F}_{sel})$ predicted by the model:

$$R^2(F_0, F_{pred}) = 1 - \frac{\sum_k (f_{0,k} - f_{pred,k})^2}{\sum_k (f_{0,k} - \frac{1}{|\mathcal{D}|} \sum_{i=1}^{|\mathcal{D}|} f_{0,i})} \tag{4.3}$$

The full IFS procedure is summarized in Algorithm 8.

To the extent of our algorithm, we run the RFS procedure on a dataset $\mathcal{TS}_{ENC}$ of four-tuples $(\tilde{s} \in \tilde{S}, a \in A, r \in \mathbb{R}, \tilde{s}' \in \tilde{S})$ built by applying the transformation ENC to the first and last elements of each four-tuple in $\mathcal{TS}$. We run the algorithm on all the state and action features but, since we assume to be working in a mono-dimensional action space, we force the action feature to always be part of the representation, so that the procedure is effectively working only on $\tilde{S}$.

At the end of the procedure, we define a simple filtering operation $RFS : \tilde{S} \to \hat{S}$ that consists in keeping only the features of $\tilde{S}$ that have been selected by the algorithm. The output of the training phase is this transformation.

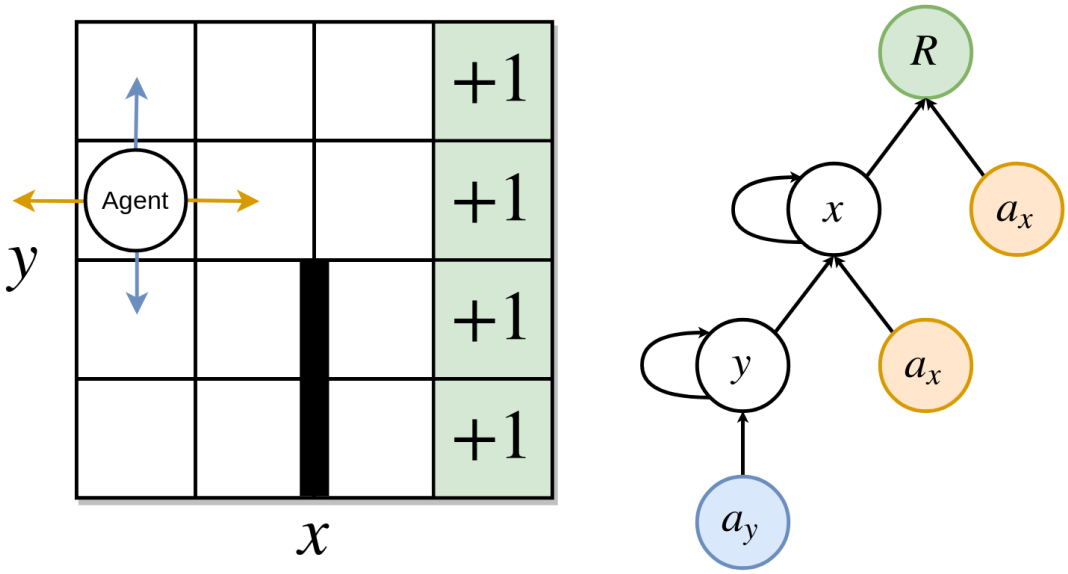

Figure 4.4: In this simple example we show the output of RFS in a simple Gridworld environment with two state features, x and y, to represent the agent's position and two action features, a_x and a_y valued in $\{-1, 0, 1\}$, to control the corresponding state features and move the agent on the discrete grid (the movement is the sum of the two effects). We use a setting with null reward everywhere except in the four goal states (green) which yield a positive reward, and a wall that cancels the effect of action a_x if the agent tries to move through it. To the right we see the dependency tree produced by RFS, which in this case selects both state features and both action features. Intuitively, the reward is explained exclusively by the state feature x and the action that controls it, a_x, because the agent gets a positive reward in each of the four cells to the far right, independently of its y coordinate, whenever it reaches one. At the same time, feature x is explained by its value and by the action feature a_x (because the next value of x is a function of both, namely $x' = x + a_x$), but also by feature y, because given the x coordinate of the agent and a direction along x we still have to know whether the agent is next to the wall in order to compute the following value of x. Finally, feature y is explained by itself and its associated action, without restrictions given by the wall.

Algorithm 8 Iterative Feature Selection (IFS)

Given: a dataset $\mathcal{D} = \langle s \in S, a \in A, s' \in S \rangle$; a target feature F_0 from the set of features of $S \cup A$
Initialize: $\mathcal{F}_{sel} \leftarrow \emptyset, \hat{F}_0 \leftarrow F_0, R^2_{old} \leftarrow 0$
repeat
  $F^* \leftarrow \arg\max_F FR(\mathcal{D}, \hat{F}_0, F)$
  if $F^* \in \mathcal{F}_{sel}$ **then**
    return $\mathcal{F}_{sel}$
  end if
  $\mathcal{F}_{sel} \leftarrow \mathcal{F}_{sel} \cup F^*$
  Build a model $\hat{f} : \mathcal{F}_{sel} \rightarrow F_0$ using $\mathcal{D}$
  $F_{pred} = \hat{f}(\mathcal{F}_{sel})$
  $\hat{F}_0 \leftarrow F_0 - F_{pred}$
  $\Delta R^2 \leftarrow R^2(\mathcal{D}, F_0, F_{pred}) - R^2_{old}$
  $R^2_{old} \leftarrow R^2(\mathcal{D}, F_0, F_{pred})$
until $\Delta R^2 < \epsilon$
return $\mathcal{F}_{sel}$

4.5 Fitted Q-Iteration

The last component of our training pipeline is the Fitted Q-Iteration algorithm (cf. Section 2.2.7). We provide as input to the procedure a new training set $\mathcal{TS}_{RFS}$ of four-tuples $(\hat{s} \in \hat{S}, a \in A, r \in \mathbb{R}, \hat{s}' \in \hat{S})$, obtained by applying the RFS transformation to the first and last elements of each four-tuple in $\mathcal{TS}_{ENC}$. We train the model to output a multi-dimensional estimate of the action-value function on $\mathbb{R}^{|A|}$, with one value for each action that the agent can take in the environment, and we restrict the output to a single value on $\mathbb{R}$ using the action identifier as index (e.g. $Q(s, 0)$ will return the first dimension of the model's output, corresponding to the value of action 0 in state s). The output of this training phase is the transformation $\hat{Q} : \hat{S} \times A \rightarrow \mathbb{R}$, which is then combined with ENC and RFS as per Equation (4.1) to produce the approximation of Q. This phase also concludes the training step.

Chapter 5

Technical Details and Implementation

In this chapter we show the implementation details of the architecture used to perform experiments. We try to provide a complete description of the parametrization of the components and of the training procedure, in order to ensure reproducibility of the experimental results.

5.1 Atari Environments

The *Arcade Learning Environment* (ALE) [3] is an evaluation platform for RL agents. ALE offers a programmatic interface to hundreds of game environments for the *Atari 2600*, a popular home video game console developed in 1977 with more than 500 games available, and is simply referred to as *Atari environments* (or *games*). We use the implementation of ALE provided by the *Gym 0.9.2* package for Python 2.7, developed by OpenAI and maintained as an open source project. This implementation provides access to the game state in the form of $3 \times 110 \times 84$ RGB frames, produced at an internal frame-rate of 60 frames per second (FPS). When an action is executed in the environment, the simulator repeats the action for four consecutive frames of the game and then provides another observation, effectively lowering the frame rate from 60 FPS to 15 FPS and making the effects of actions more evident (Figure 5.1).

We perform a preprocessing operation on the states similar to that performed by Mnih et al. in DQN [32], in order to include all necessary information about the environment and its nominal dynamics in the new state representation. First we convert each RGB observation to a single-channel grayscale representation in the discrete 8-bit

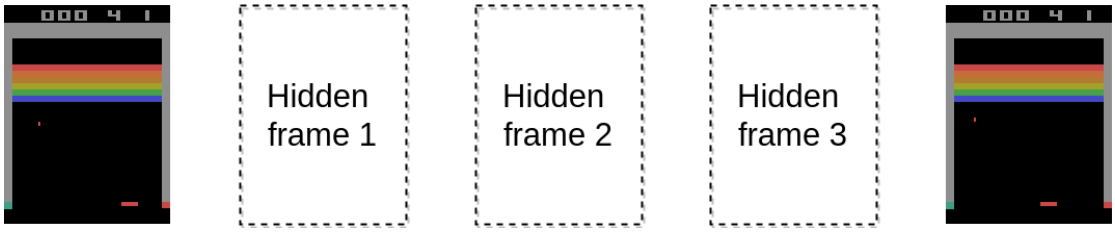

Figure 5.1: Sampling frames at a frequency of $\frac{1}{4}$ in Breakout.

interval $[0, 255]$ using the *ITU-R 601-2 luma transform*:

$$L = \frac{299}{1000}R + \frac{587}{1000}G + \frac{114}{1000}B \tag{5.1}$$

where R, G, B are the 8-bit *red, green* and *blue* channels of the image. We then normalize these values in the $[0, 1]$ interval via *max-scaling* (i.e. dividing each pixel by 255). Moreover, we define a rounding threshold v_{round} specific to each game and we round all pixel values above or below the threshold to 1 or 0 respectively, reducing the images to a 1-bit color space in order to facilitate the training of the AE. We also reduce the height of the image by two pixels in order to prevent information loss due to a rounding operation performed by the convolution method used in the AE. Finally, we concatenate the preprocessed observation to the last three preprocessed frames observed from the environment, effectively blowing up the state space to a $4 \times 108 \times 84$ vector space (Figure 5.2). The initial state for an episode is artificially set as a repetition of the first observation provided by the simulator. This operation is needed to include all necessary information about the environment's nominal dynamics in the state space used for training, so that the AE will be able to extract them in the representation.

Moreover, in order to facilitate comparisons and improve stability, we remain loyal to the methodology used for DQN and perform the same clipping of the reward signal in a $[-1, 1]$ interval.

We also add a tweak to the Gym implementation of ALE in order to fix a requirement of some environments of performing some specific actions in order to start an episode (e.g. in *Breakout* it is required that the agent takes action 1 to start the game). We automatically start each episode by randomly selecting one of the initial actions of the game and forcing the agent to take that action at the beginning of the episode.

Finally, for those games in which the agent has a lives count, we monitor the number of remaining lives provided by the simulator in the *ale.lives* parameter. For those (s, a, r, s') transitions in which the agent loses a life, we consider s' as a terminal state, so that the FQI update will only use the reward rather than the full value.

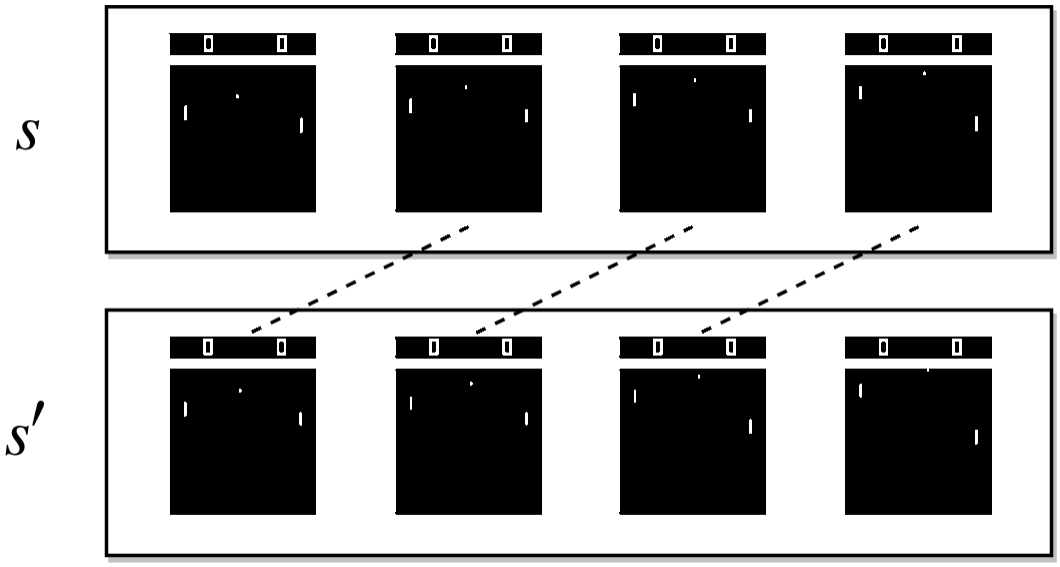

Figure 5.2: Two consecutive states s, s' in Pong, after the preprocessing operation. Each binary image in a sequence of four is an observation of 108×84 pixels, and the full $4 \times 108 \times 84$ tensor is given as input and target to the AE. Notice that between the two consecutive states there are three frames in common, with the newest observation appended as last frame in s' and the oldest being pushed out.

Type	Input	Output	# Filters	Filter	Stride	Activation
Conv.	$4 \times 108 \times 84$	$32 \times 26 \times 20$	32	8×8	4×4	ReLU
Conv.	$32 \times 26 \times 20$	$64 \times 12 \times 9$	64	4×4	2×2	ReLU
Conv.	$64 \times 12 \times 9$	$64 \times 10 \times 7$	64	3×3	1×1	ReLU
Conv.	$64 \times 10 \times 7$	$16 \times 8 \times 5$	16	3×3	1×1	ReLU
Flatten	$16 \times 8 \times 5$	640	-	-	-	-
Reshape	640	$16 \times 8 \times 5$	-	-	-	-
Deconv.	$16 \times 8 \times 5$	$16 \times 10 \times 7$	16	3×3	1×1	ReLU
Deconv.	$16 \times 10 \times 7$	$64 \times 12 \times 9$	64	3×3	1×1	ReLU
Deconv.	$64 \times 12 \times 9$	$64 \times 26 \times 20$	64	4×4	2×2	ReLU
Deconv.	$64 \times 26 \times 20$	$32 \times 108 \times 84$	32	8×8	4×4	ReLU
Deconv.	$32 \times 108 \times 84$	$4 \times 108 \times 84$	4	1×1	1×1	Sigmoid

Table 5.1: Layers of the autoencoder with key parameters.

5.2 Autoencoder

We use the autoencoder to extract a high level representation $\tilde{S}$ of the state space in an unsupervised fashion. We structure the AE to take as input the preprocessed observations from the environment and predict values on the same vector space. The first four convolutional layers make up the encoder and perform a 2D convolution with the *valid* padding algorithm, such that the input of each layer (in the format $channels \times height \times width$) is reduced automatically across the last two dimensions (height and width) according to the following formula:

$$output_i = \lfloor (input_i - filter_i + stride_i)/stride_i \rfloor \tag{5.2}$$

Since the main purpose of pooling layers is to provide translation invariance to the representation of the CNN (meaning that slightly shifted or tilted inputs are considered the same by the network), here we choose to not use pooling layers in order to preserve the precious information regarding the position of different elements in the game; this same approach was adopted in DQN. A final *Flatten* layer is added at the end of the encoder to provide a 1D representation of the feature space, which is reversed before the beginning of the decoder. The decoder consists of deconvolutional layers with symmetrical filter sizes, filter numbers, and strides with respect to the encoder. Here the *valid* padding algorithm is inversed to expand the representation with this formula:

$$output_i = \lfloor (input_i \cdot stride_i) + filter_i - stride_i \rfloor \tag{5.3}$$

A deconvolutional layer is added at the end to reduce the number of channels back to the original four, without changing the width and height of the frames (i.e. using unitary filters and strides). All layers in the AE use the *Rectified Linear Unit* (ReLU) [34, 26] nonlinearity as activation function, except for the last layer that uses *sigmoids* to limit the activations values in the same $[0, 1]$ interval of the input (Figure 5.3). Details of the AE layers are summarized in Table 5.1.

We train the AE with the Adam optimization algorithm [25] (see Table 5.2 for details on the hyperparameters) set to minimize the *binary cross entropy* loss defined as:

$$L(y, \hat{y}) = -\frac{1}{N}\sum_{n=1}^{N}[y_n log(\hat{y}_n) + (1 - y_n) log(1 - \hat{y}_n)] \tag{5.4}$$

where y and $\hat{y}$ are vectors of N target and predicted observations in the state space. The dataset used for training is built from the dataset collected for the whole learning procedure described in Algorithm 6, taking only the first elements of the four-tuples $(s, a, r, s') \in \mathcal{TS}$ (which are used as input and targets). We prevent *overfitting* of the training set by monitoring the performance of the AE on a held-out set of validation samples that amounts to roughly 10% of the training data, and stopping the procedure when the validation loss does not improve by at least 10^{-5} for five consecutive training epochs.

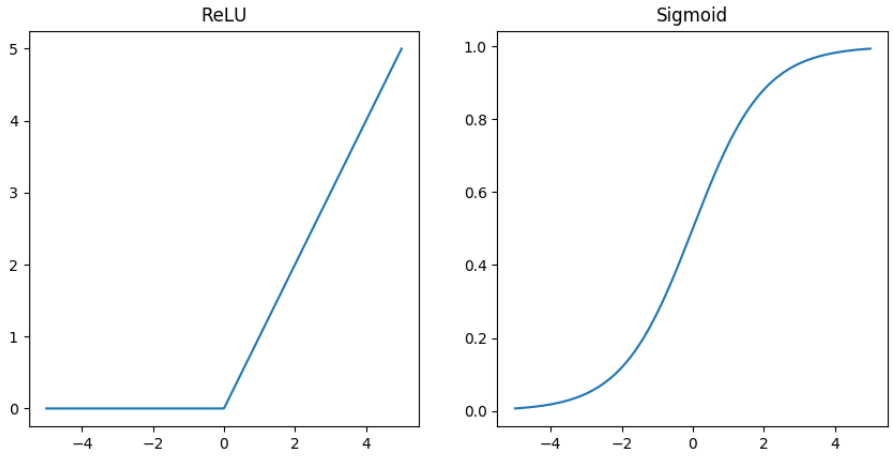

Figure 5.3: The ReLU and Sigmoid activation functions for the AE.

Parameter	Value
Learning rate	0.001
Batch size	32
Exponential decay rate (β_1)	0.9
Exponential decay rate (β_2)	0.999
Fuzz factor (ε)	10^{-8}

Table 5.2: Optimization hyperparameters for Adam.

Parameter	Value
M (Number of base estimators)	50
K (Number of randomly selected attributes)	All available attributes
Scoring method	Variance reduction
Max tree depth	None
n_{min} (node)	5
n_{min} (leaf)	2

Table 5.3: Parameters for Extra-Trees and its base estimators in RFS.

Parameter	Value
K (for K-fold cross-validation)	3
ξ (significance)	0.95

Table 5.4: Parameters for RFS.

5.3 Tree-based Recursive Feature Selection

We use the RFS algorithm to reduce the state space representation computed by the AE down to the feature space $\hat{S}$. We base both the feature ranking method FR and the model $\hat{f}$, used for computing the descriptiveness of the features, on the supervised Extra-Trees algorithm (cf. Section 2.3.2).

The feature ranking approach with Extra-Trees is based on the idea of scoring each input feature by estimating the variance reduction produced anytime that the feature is selected during the tree building process. The ranking score is computed as the percentage of variance reduction achieved by each feature over the M trees built by the algorithm.

At the same time, Extra-Trees is a sufficiently powerful and computationally efficient supervised learning algorithm to use as $\hat{f}$. Note that in general FR and $\hat{f}$ could be different algorithms with different parametrizations, but Castelletti et al. use the same regressor for both tasks (as does the code implementation of RFS and IFS that we used for experiments), and we therefore complied with this choice. The parametrization of Extra-Trees for FR and $\hat{f}$ is reported in Table 5.3[1] (cf. Section 2.3.2).

We use the R^2 metric defined in Equation (4.3) to compute the ability of the selected features to describe the target, in K-fold cross validation over the training set $\mathcal{D}$. We compute a confidence interval over the scores of the validation predictions as:

$$CI = \sqrt{\frac{1}{|\mathcal{D}|}\sum_{i=1}^{|\mathcal{D}|}(R^2)^2 \cdot (\frac{1}{|\mathcal{D}|}\sum_{i=1}^{|\mathcal{D}|}(R^2))^2} \tag{5.5}$$

and we adapt the stopping condition of RFS by setting $\epsilon = CI + CI_{old}$ (where the suffix *old* has the same meaning as in Algorithm 8) so that the condition becomes $R^2 - CI < R^2_{old} - CI_{old}$. We also multiply ϵ by a *significance* factor ξ in order to control the amount of variance that a feature must explain in order to be added to the selection: higher values of ξ mean that the selection will yield a smaller subset composed exclusively of very informative features (even if the overall amount of variance explained is not necessarily the whole possible amount). The hyperparameters used for RFS are reported in Table 5.4.

[1] Note that we use two different values for the minimum number of samples required to split an internal node or a leaf.

Parameter	Value
M (Number of base estimators)	100
K (Number of randomly selected attributes)	All available attributes
Scoring method	Variance reduction
Max tree depth	None
n_{min} (node)	2
n_{min} (leaf)	1

Table 5.5: Parameters for Extra-Trees and its base estimators in FQI.

5.4 Tree-based Fitted Q-Iteration

We use the FQI algorithm to learn an approximation of the Q function from the compressed and reduced state space extracted by the previous two modules. For consistency with the feature selection algorithm, we use the Extra-Trees learning method as function approximator for the action-value function. The model is trained to map the 1D compressed feature space $\hat{S}$ to the $|A|$-dimensional action-value space $\mathbb{R}^{|A|}$, and we use the action identifiers to select the single output value of our approximated $\hat{Q}$ function. The parametrization for Extra-Trees is reported in Table 5.5 (cf. Section 2.3.2).

Since the FQI procedure introduces a small bias to the action-value estimate at each iteration (due to approximation errors), we implement an *early stopping* procedure based on the evaluation of the agent's performance. Every fixed number of iterations, we evaluate the performance of an ε-greedy policy (with $\varepsilon = 0.05$) based on the current partial approximation $\hat{Q}_i$, by composing all the modules in the pipeline to obtain the full Q as per Equation (4.1). If the agent's performance does not improve for five consecutive evaluations, we stop the training and produce the best performing estimation as output to the training phase. The performance is evaluated by running the policy for five episodes and averaging the clipped cumulative return of each evaluation episode.

Finally, we consider a discount factor $\gamma = 0.99$ for the MDP in order to give importance to rewards in a sufficiently large time frame.

5.5 Evaluation

An evaluation step is run after each training step of the full procedure. Similarly to what we do to evaluate the agent's performance during the training of FQI, here we use an ε-greedy policy with $\varepsilon = 0.05$ based on the full Q composition of Equation (4.1). The reason for using a non-zero exploration rate during evaluation is that ALE provides a fully deterministic initial state for each episode, and by using a deterministic policy we would always observe the same trajectories (thus making it impossible to evaluate the Q-value in those state-action pairs that the agent never explores). Using a non-zero

exploration rate allows us to assess the agent's capability of playing effectively in any state of the game, and of correcting its behavior after an (albeit artificial) mistake.

We let the agent experience N separate episodes under the ε-greedy policy, and for each episode we consider the cumulative clipped return and the number of steps occurred. The mean and variance of these two metrics across the N episodes provide us with insights on the agent's performance: a high average return obviously means that the algorithm has produced a good policy, but at the same time a low variance in the number of steps could indicate that the agent is stuck in some trivial policy (e.g. to take always the same action) which causes the episodes to be essentially identical, even accounting for the non-zero exploration rate. The latter aspect, while not negative in general, can help in the initial steps of experiments to detect potential problems in the implementation.

Evaluation parameters are summarized in Table 5.6.

Parameter	Value
Exploration rate ε	0.05
N	10

Table 5.6: Parameters for evaluation.

Chapter 6

Experimental Results

In this chapter we show experimental results of our algorithm on some Atari games. We show that the representation of the states learned by our feature extraction pipeline is suitable for the semi-batch control approach with FQI, and that our agent is able to learn non-trivial policies with good sample efficiency on different environments.

6.1 Premise

Our approach aims at optimizing sample efficiency, but does not account for the computational complexity of training and evaluating the full pipeline. All three main components of the algorithm benefit a great deal from parallel computing, to the point where the hardware itself is a key component in making the algorithm treatable at all. We were thus strongly limited in our experimental phase by our access to hardware for heavy parallel computing, with even costs for renting servers on cloud providers being prohibitive when considering our runtime. We therefore had to be extremely selective in what experiments to run, each of which took days at a time, and well balanced between exploring new possibilities (hyperparameters, network architectures, environments) and evaluating current configurations. In this chapter we report the best findings across all our experiments and we try to outline the thought process that led us to favor some choices over others. The hardware configurations of the three servers that we used for experiments is reported in Table 6.1.

The code implementation of the algorithm was based on Python 2.7 and its *de facto* standard libraries for general machine learning, GPU-based deep learning, and linear algebra. We trained and used the AE on an *Nvidia Tesla K40C* GPU, using the *Keras 2.0.6* API as interface to the *Tensorflow 1.3.0* library for deep learning, whereas the training and evaluation of Extra-Trees for RFS and FQI were run on CPU using the *Scikit-Learn 0.19.0* library. We used the implementations of FQI and RFS provided in

Server ID	vCPU count	GPU	RAM (GB)
#1	64	None	252
#2	8	1× Nvidia Tesla K40C	32
#3	4	1× Nvidia Tesla K40C	32

Table 6.1: Server configurations for experiments.

the open source *IFQI* library by Matteo Pirotta. Finally data manipulation and any other algebraic operations were done with *Numpy 1.13.1*.

6.2 Baseline

To evaluate the results of our approach with respect to other algorithms, we compared our agent's performance with that of DQN [32] and of a fully random policy. For DQN, we used an open source implementation of the paper by Mnih et al. with the same exact parametrization, and run the algorithm for a total of 50 million online training samples on the *Breakout, Pong*, and *Space Invaders* environments from the Atari games. To remain loyal to the original DQN methodology, we run an evaluation phase of 125000 steps every 250000 collected training samples, and we considered the average cumulative non-clipped reward across the episodes completed in this period. A similar evaluation was also run once on the fully random policy. The best performance achieved by the baseline algorithms is reported in Table 6.2, and we show the learning curve of DQN across the 50 million frames in Figures 6.1, 6.2 and 6.3.

Environment	$\|A\|$	Random	Best DQN	Samples for best DQN
Breakout	4	1.09	319.83	≈ 19250000
Pong	6	-20.49	19.82	≈ 35250000
Space Invaders	6	174.46	1125.41	≈ 31500000

Table 6.2: Average performance of baseline algorithms.

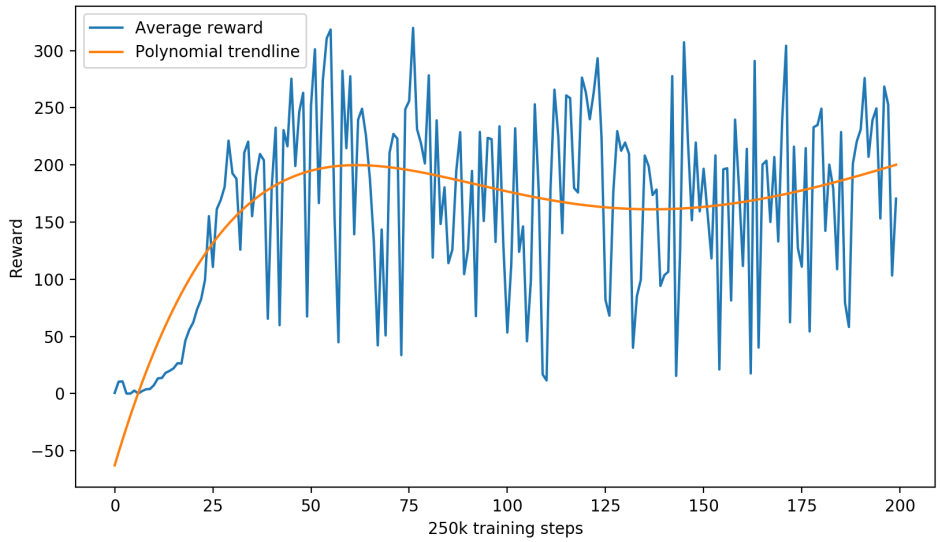

Figure 6.1: Average evaluation reward of DQN in Breakout (each point is the average score over 125000 *evaluation steps).*

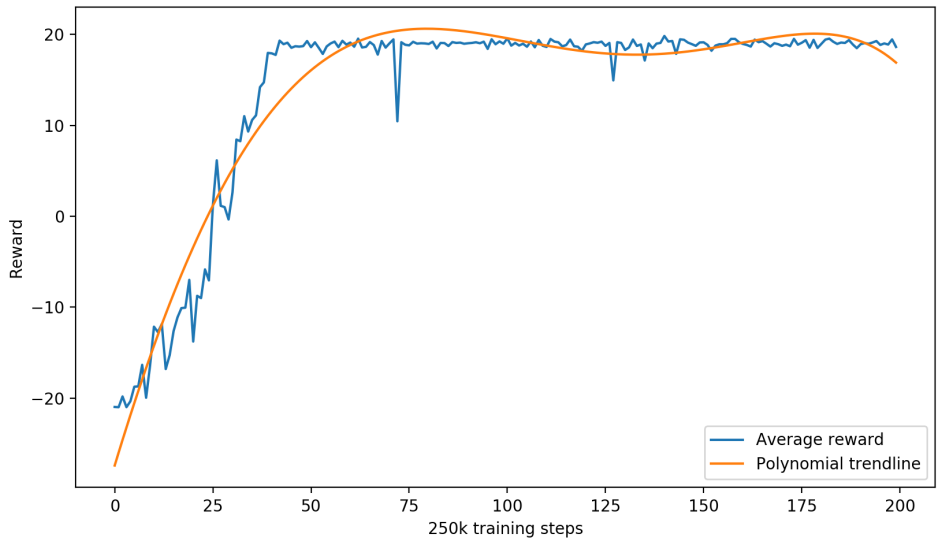

Figure 6.2: Average evaluation reward of DQN in Pong (each point is the average score over 125000 *evaluation steps).*

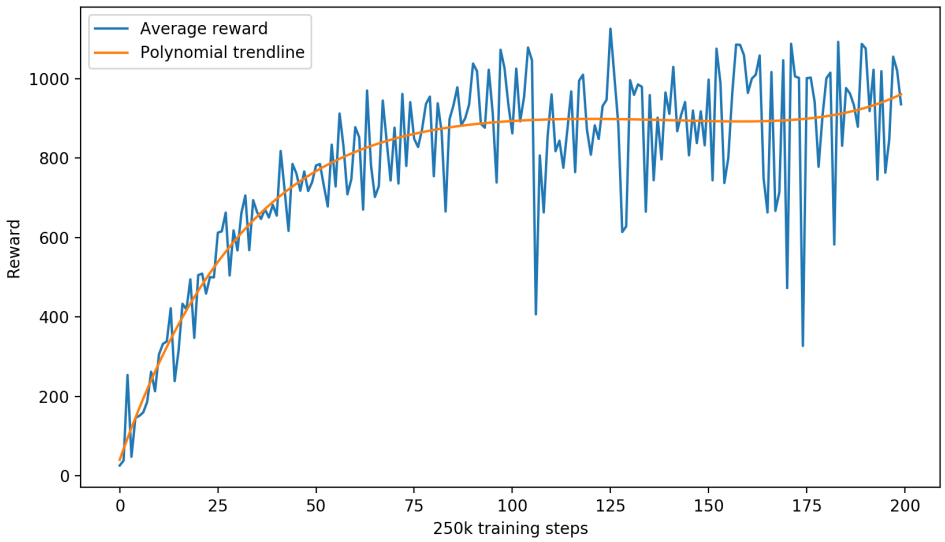

Figure 6.3: Average evaluation reward of DQN in Space Invaders (each point is the average score over 125000 *evaluation steps).*

6.3 Autoencoder

Due to the extremely high training and (especially) evaluation times that we encountered in FQI[1], and the almost intractable runtime of RFS[2], we had to formally assess the suitability of the extracted features for control problems before moving on to training the other components in the pipeline. To do so, we run a series of tests devised to highlight different aspects of success in the feature extraction. Once a training configuration was deemed satisfactory, we kept it fixed for all the following experiments.

The most simple test that we run consisted in assessing the reconstruction loss and accuracy of the AE on a held-out validation set (cf. Section 5.2). We were able to achieve very high reconstruction accuracy in all environments, with no sensible differences between training sets collected under different exploration rates. In Table 6.3 we report validation performance of the AE on datasets of ≈ 50000 samples collected with different values of ε (see also Figures 6.4, 6.5, and 6.6). In general, the reconstruction of the AE is better when the training dataset is collected under a high exploration rate. This is

[1]Slow performance in evaluation is due to the sample-wise forward prediction across the full pipeline required at each step of evaluation episodes. Specifically, each prediction of the Q function needs a forward pass of the 4-layer encoder (which requires loading data in the GPU) and a forward pass of Extra-Trees (which due to an internal inefficiency in *Scikit-learn* was extremely slow when predicting on a single sample).

[2]Which can take more than a week to complete, on our most performing server.

Environment	ε	Val. loss	Val. accuracy
Breakout	1.0	$\approx 10^{-5}$	1.0
	0.55	$\approx 10^{-4}$	0.9999
	0.1	$\approx 10^{-4}$	0.9997
Pong	1.0	$\approx 10^{-4}$	0.9999
	0.55	$\approx 10^{-4}$	0.9997
	0.1	$\approx 10^{-4}$	0.9993
Space Invaders	1.0	$\approx 10^{-3}$	0.9987
	0.55	$\approx 10^{-3}$	0.9985
	0.1	$\approx 10^{-3}$	0.9978

Table 6.3: Validation performance of our AE on fully random datasets of ≈ 50000 samples.

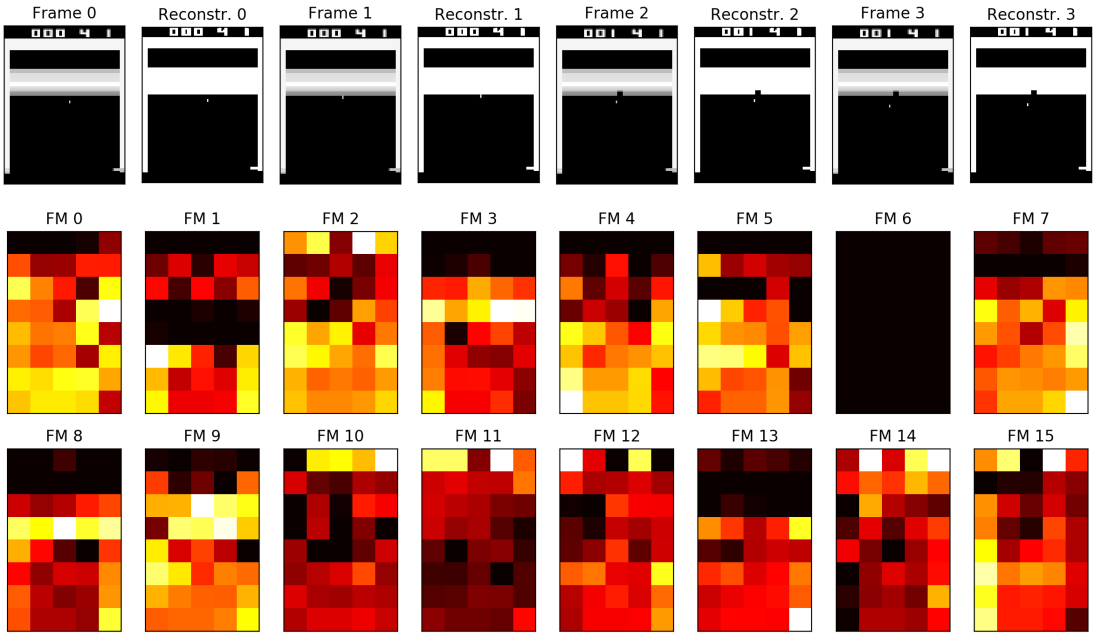

Figure 6.4: AE reconstruction and feature maps on Breakout. Each pair in the top row shows a frame of a 4-channel state s given as input to the AE, with its associated reconstructed channel. The bottom two rows show the relative activation values of the innermost feature maps before the flatten layer, after encoding s: colors represent a heatmap from black (0) to white (map-wise maximum activation value). The same applies to Figures 6.5 and 6.6.

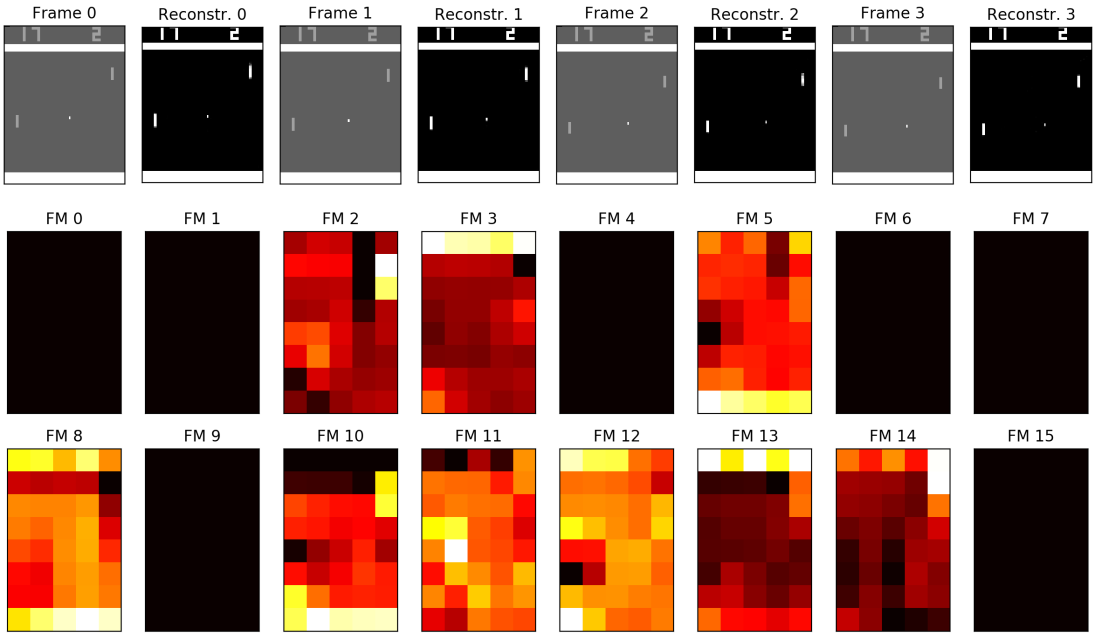

Figure 6.5: AE reconstruction and feature maps on Pong.

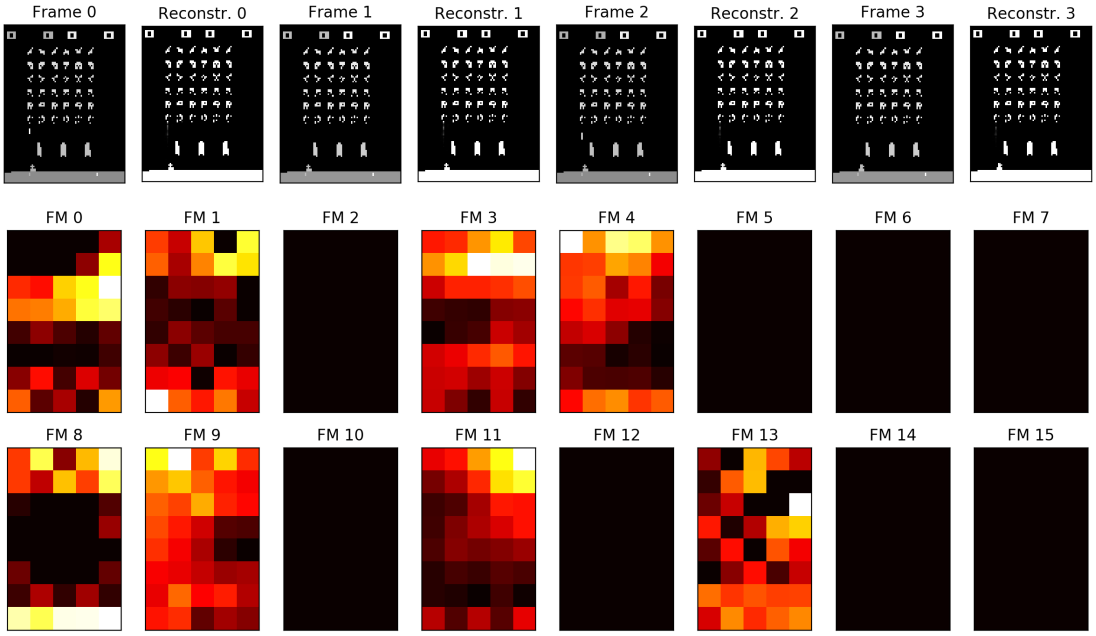

Figure 6.6: AE reconstruction and feature maps on Space Invaders. Note that the lower accuracy here translates to a poor definition in reconstructing moving elements like the player's character and projectiles.

Environment	ε	R^2	MSE
Breakout	1.0	0.937	0.0272
	0.55	0.854	0.0761
	0.1	0.855	0.0748
Pong	1.0	0.945	0.0167
	0.55	0.849	0.0334
	0.1	0.905	0.0241
Space Invaders	1.0	0.532	0.3895
	0.55	0.468	0.5032
	0.1	0.457	0.5126

Table 6.4: Results of the $\tilde{S}$-Q mapping experiment with different exploration rates to collect the datasets.

intuitively due to the fact that more random policies are less effective and can only reach a few states, so that the AE has to learn a simpler representation of the environment (e.g. there is no point in learning to reconstruct the higher layers of the wall in Breakout if the agent never breaks them). This does not apply to environments like Pong, in which the agent has no effect on the fixed elements of the game, and for which we see an almost constant reconstruction accuracy with all exploration rates. Less formally, a visual inspection of the reconstruction helped us in the early experimental phases and highlighted how even a small change in accuracy (in the order of 10^{-3}) could result in an incredibly noisy output. This can be seen in Figure 6.6, where a 99.8% reconstruction accuracy on Space Invaders means that the AE is not able to reconstruct some small moving elements of the game.

At the same time, we also inspected the values and behaviors of the features maps produced by the encoder before flattening, by creating short animations (See Figures 6.4, 6.5, and 6.6) of how the activation values changed in a sequence of about a hundred states. This confirmed that the extracted features maps contained abstract enough information (without excessive spatial correlation between the features). We also observed that in Space Invaders, on average, almost half of the features *died*. This phenomenon is a common occurrence in CNNs that use the ReLU activation function (due to the fact that ReLU has a null gradient for all inputs lower or equal than zero, cf. Figure 5.3), but we were not able to explain such a high death rate on this particular environment, which presents a more complicated structure than the other environments that we tested.

In order to truly assess the compatibility of the extracted features with control problems, we also trained a supervised model to learn the Q approximation produced by DQN using the extracted features (we call this an $\tilde{S}$-Q *test*). We used a training set composed of tuples $(ENC(s) \in \tilde{S}, q \in \mathbb{R}^{|A|})$, where s is a state from the environment, after the preprocessing described in Section 5.1, and q is the $|A|$-dimensional estimate

produced by DQN when it receives s as input. Note that we could use the same input for both networks, because the preprocessing that we perform on the observations before feeding a sample to the encoder (cf. Section 5.1) is basically the same that is applied to the inputs for DQN. To account for the slight different preprocessing, we computed q before applying the transformations which are unique to our preprocessing, namely the binarization and cropping. For each environment, we used the best performing DQN (as per Section 6.2) to produce the targets, and we sampled ≈ 50000 states from the same dataset on which the AE was trained. To learn the Q approximation, we used the same Extra-Trees model and hyperparameters that we use for FQI (See Table 5.5), to ensure that the configuration itself was adequate to describe the nonlinear relations between the features and the action-value function at convergence of FQI. This was done by simply fitting the model on the $(ENC(s), q)$ pairs, and evaluating the R^2 score (cf. Definition (4.3)) and *Mean Squared Error* (MSE) of the predictions on a held-out validation set of roughly 5% of the training samples. As seen in Figure 6.7, the extracted features are suitable for describing the Q function learned by DQN with a good degree of precision, and constitute an adequate base for our whole approach. We were able to obtain an average R^2 score of 0.88, 0.90, and 0.48 on all three tested environments respectively. Similarly to what we observed for the AE, in Space Invaders we have a drop in performance probably due to a difficulty in representing all elements in the environment. For instance, since the AE is not able to properly represent the character and its projectiles, we can assume that there are no features that describe these elements. However, these are essential to predict the reward and, consequently, the Q function, and their absence could explain the bad prediction. We report the results of these tests, run on datasets collected with different values of ε at different iterations of our full algorithm, in Table 6.4.

6.4 Recursive Feature Selection

The main purpose of RFS in our learning pipeline is to provide a fast forward propagation of the AE at control time, by keeping only the AE weights that are essential for the representation. The runtime of RFS, however, is the longest amongst the three main components, taking up to a week to complete and extending the runtime of the full algorithm to a point where it becomes unfeasible. We therefore had to ignore RFS during most of our experiments, resorting to only running it once per environment using a dataset collected under a fully random policy and an AE trained on the same dataset (as if we were running the selection at the first step of the main procedure). At the same time, we found it appropriate to run another simple feature selection technique which consisted in only keeping those features with nonzero variance (NZV), in order to simplify our feature space without losing information. We found that RFS reduced the representation by up to 60% with respect to NZV on Pong, which indicates that the AE

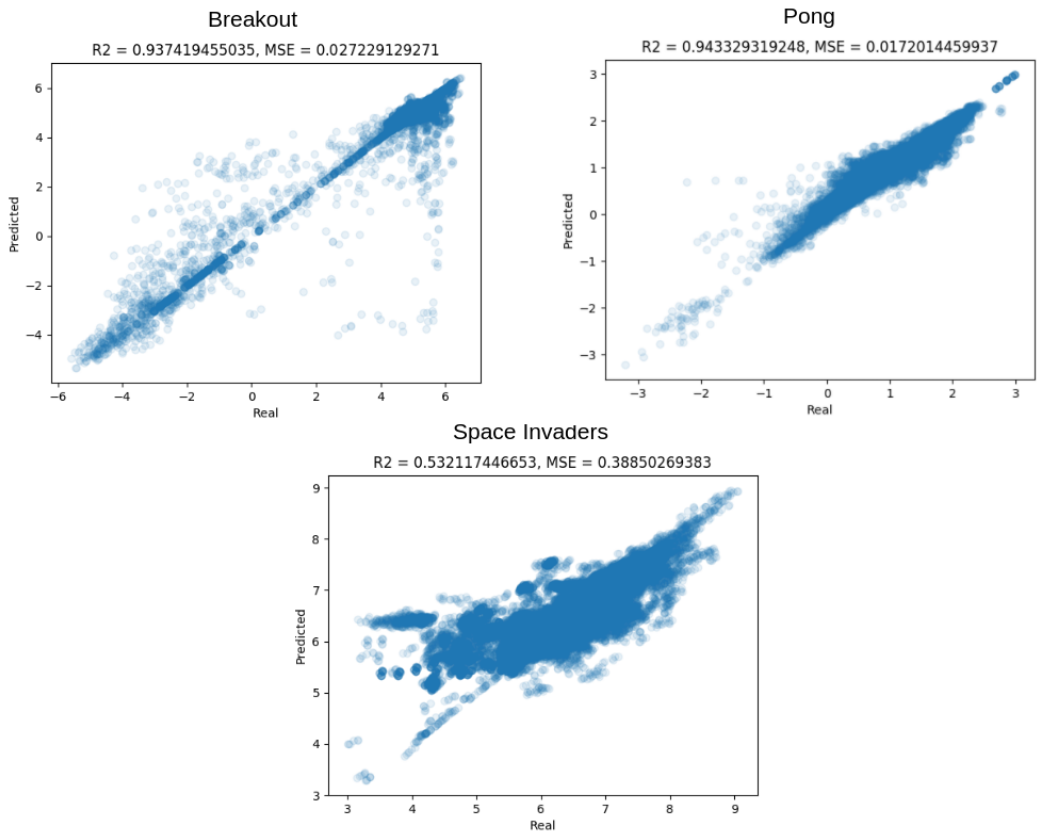

Figure 6.7: Values predicted by the supervised model in the $\tilde{S}$-Q test vs. real values predicted by DQN. Note that the $|A|$-dimensional estimate of the Q function is flattened and treated as a sequence of $|A|$ independent values in order to plot it.

Environment	Original	NZV	RFS	Action selected (RFS)
Breakout	640	599	4	No
Pong	640	585	245	Yes
Space Invaders	640	320	640	Yes

Table 6.5: Number of features kept by the two feature selection techniques that we used in our experiments, run on datasets of 100000 *samples collected under a fully random policy.*

Environment	Score	Step	ε	FQI epoch
Breakout	17	2 of 3	0.55	400
Pong	-9	2 of 3	0.55	350
Space Invaders	460	2 of 3	0.55	450

Table 6.6: Best average performance reached by our agent on different environments.

does indeed extract a great deal of redundancy that can be ignored for control purposes. However, we were not able to replicate this performance on the other two environments. In Breakout, RFS only selected four state features and did not select the action. On the other hand, this behavior was inverted on Space Invaders, where the procedure selected all state and action features (including those with zero variance removed by NZV) at the first step, when explaining the reward. The reason for this inconsistent behavior by RFS is probably due to an incompatibility between the RFS procedure itself and the dynamics of the features extracted by the AE but, as we will show in the following sections, this does not prevent the agent from learning a good policy using the AE's representation. In Figures 6.8 and 6.9, we show the feature dependency trees built by RFS on Breakout and Pong (we omit the tree from Space Invaders because it is of little informative value).

6.5 Fitted Q-Iteration

The final part of our experimental methodology consisted in running the full learning pipeline as described in Algorithm 6, and evaluating the performance of our algorithm in terms of average reward as we did for DQN and the random policy in Section 6.2. As we mentioned in the previous section, due to the excessively long computational times of RFS we chose to remove the module entirely from the pipeline, resorting to simply keeping those features with nonzero variance across the dataset. At the same time, we also had to deal with the long runtime for the evaluation of the policy during training of FQI (necessary for early stopping), due to a general computational complexity of our Q approximation itself, and to an internal inefficiency in the software library that we used for Extra-Trees. We tried to address this issue by training FQI for 50 iterations at a

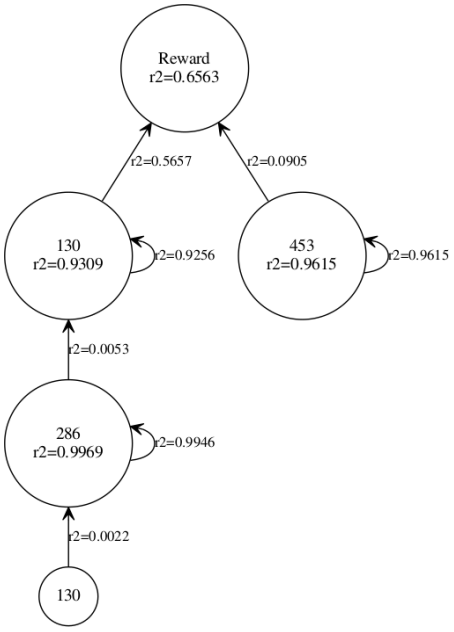

Figure 6.8: RFS dependency tree in Breakout. Note how the procedure in this case is not able to correctly understand the dynamics of the environment and only keeps four state features without even keeping the action, indicating that in this case the features extracted by the AE are not suitable for control-oriented selection.

time before evaluating the current policy, for a total of 20 overall evaluations across 1000 training iterations. This resulted in a noisy evaluation performance, but no more noisy than when we tested the policy at each iteration. We also had to face computational complexity when deciding how many steps of the main algorithm to run. We decided to use a custom φ function to reduce ε (cf. Section 4.2) dependent on the total number of steps, so that ε would reach ε_{min} at the last iteration, and at each step would decrease by a fixed quantity as follows:

$$\varphi(\varepsilon) = \varepsilon - \frac{1 - \varepsilon_{min}}{I} \tag{6.1}$$

where I is the total number of iterations (note that the rule only applies if ε is greater that ε_{min}). We run a comparison of different values of ε at different steps of the procedure, and we eventually decided to settle for running three iterations ($I = 3$) with $\varepsilon_{min} = 0.1$, so that we used the values $\varepsilon = 1$, $\varepsilon = 0.55$ and $\varepsilon = 0.1$ in sequence. This resulted in a tractable runtime for the full algorithm (however still in the order of days) and an overall good variety in exploration.

Since the main focus of our work was to minimize the number of training samples, we empirically tried different sizes for the training sets collected at each step. We started from a conservative size of 1 million samples, and gradually reduced this amount while

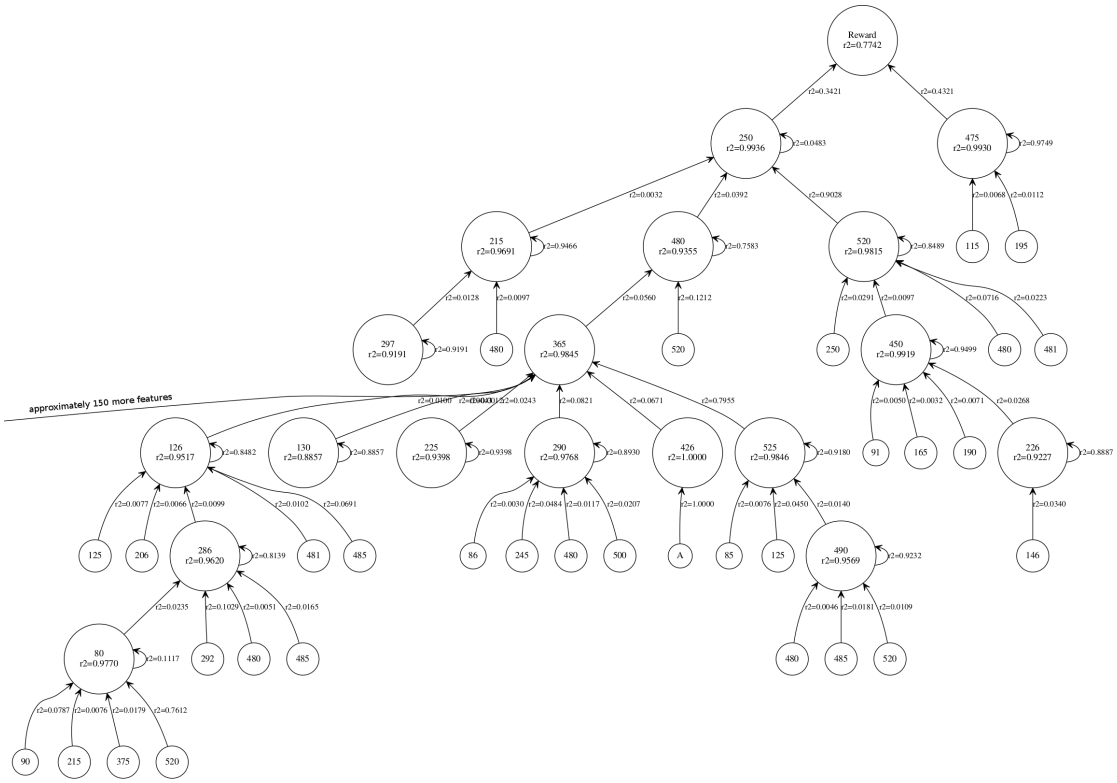

Figure 6.9: RFS dependency tree in Pong (showing only topmost 50 nodes).

Environment	Random	Our best	Best DQN	Score ratio (ours v. DQN)
Breakout	1	17	**319**	0.05
Pong	−20	−9	**19**	0.3
Space Invaders	174	460	**1125**	0.4

Table 6.7: Best average performance of our algorithm compared to the baseline algorithms. Note that the score in Pong is shifted to a $[0, 42]$ *range to compute the score ratio.*

Environment	Samples	Our best	DQN	Sample ratio	Score ratio
Breakout	100000	**17**	2	0.005	8.5
Pong	100000	**-9**	−20	0.002	12
Space Invaders	100000	**460**	145	0.003	3.17

Table 6.8: Best average performance reached by our algorithm compared with the best average performance of DQN using the same number of collected samples. Sample ratio is computed using the number of samples required by DQN to reach its best performance as reported in Table 6.2. Note that the score in Pong is shifted to a $[0, 42]$ *range to compute the score ratio.*

monitoring the agent's top performance. We were not able to notice a sensible difference between any dataset size above 50000, so we eventually settled for this amount and kept it fixed during experiments.

Moving on to the main results of the FQI training, we report in Tables 6.6, 6.7, and 6.8 the performance of our algorithm. In Table 6.6, we show the best average evaluation score achieved by our agent during the main training procedure. We note that FQI benefits a great deal by a sufficiently high exploration rate, with peak performance typically reached at $\varepsilon \approx 0.5$ (this result was often observed during experiments, even with different configurations for the AE and FQI). Despite being an expected result due to the fact that FQI needs to learn at once both the value of good and poor states, unlike online neural algorithms like DQN that can exploit an intrinsic memory of the architecture to store information about previous samples, this also meant that we only reached peak performance with our agent at the second main step, with $\varepsilon = 0.55$. We found that this result was consistent throughout our tests, and we also partly attribute to this aspect the inferior performance of our methodology with respect to the state of the art, because we could never properly exploit the learned knowledge to explore the environment to the required degree. Our agent could consistently achieve a non-trivial performance on all environments nonetheless, as reported in Table 6.7, reaching on average 25% of DQN's score.

However, despite these poor general results we were able to achieve our main objective of sample efficiency. Our agent was consistently able to outperform DQN when considering the amount of samples collected by our procedure to reach its best performance. In Table 6.8, we show how the performance of our algorithm at its best is on

average almost eight times better than DQN after collecting the same amount of samples (roughly 100000). At the same time, even if our best scores amounted to at best 40% of DQN's score, we were able to achieve them with as little as 0.2% of the collected samples (cf. Table 6.8).

Chapter 7

Conclusions and Future Developments

In this work we presented a modular deep reinforcement learning procedure with the objective of improving the sample efficiency of this class of algorithms. The main reason to explore the potential of our approach is to apply control algorithms to those problem with a big state space, and from which it is difficult or expensive to collect samples for learning.

We combined the feature extraction capabilities of unsupervised deep learning and the control-oriented feature selection of RFS, in order to reduce the pixel-level state space of Atari games down to a more tractable feature space of essential information about the environment, from which we then learned a control policy using the batch reinforcement learning FQI algorithm. Our autoencoder was able to achieve good reconstruction accuracy on all the environments, and we manged to extract a representation of the state spaces which proved to be suitable for approximating the optimal action-value function. Due to a limit of the computational power that we had available during the experimental phase, we were not able to explore the capabilities of RFS fully, and we had to remove it from the pipeline without being able to compare the performance of our algorithm before and after reducing the feature space. The only experiments that we were able to run on RFS provided us with mixed information, reducing the state space as expected on some environments but failing completely on others. The training of FQI on the feature space resulted in a sub-optimal performance, and highlighted an intrinsic inefficiency in our semi-batch approach, but we were nonetheless successful in reaching our objectives.

Our algorithm proved to be less powerful than DQN in learning an optimal control policy on the environments we tested, as our agent was never able to surpass the scores of DeepMind's algorithms. However, we were able to obtain a good sample efficiency,

which allowed our agent to learn good policies using as little as 50000 samples, surpassing the performance of DQN by eight times on average when comparing the two methods using the same amount of samples that our agent required to get to its best performance. Moreover, when considering the ratio between the performance of the two algorithms, and the ratio of the samples collected by both algorithms to achieve their top performance, we showed that the relative difference in performance is smaller by two orders of magnitude than the relative difference in collected samples, as we were able to achieve on average 25% of DQN's score using as little as 0.2% of the samples. Our algorithm makes a step towards a more sample-efficient DRL, and to the best of our knowledge would be a better pick than DQN in settings characterized by a lack of training samples and a big state space. The sub-optimal performance reached by our agent only encourages us to explore the possibilities of our algorithm further.

7.1 Future Developments

We extended the work by Lange and Riedmiller [27] to cover more complex environments, and we tried to deviate as little as possible from the methodology of Mnih et al. in DQN in order to facilitate comparison. However, we feel that our research is far from complete, and in this section we propose some paths on which we would like to continue.

First of all, in the light of the recently published work by Higgins et al. [23] on control-oriented feature extraction using autoencoders, we propose to apply β *Variational Autoencoders* (β-VAE) [24, 22] instead of the purely convolutional AE presented in this work (more similar to the DQN methodology), with the aim of extracting disentangled features that are associated almost one-to-one with specific elements in the environments. A second approach that we briefly explored during the writing of this thesis consisted in training the AE in an almost supervised way, using the states of the environment as input and the following states as output. This would change the extracted feature space to account for the full dynamics of the environment (rather than simply the nominal dynamics that we considered by stacking consecutive observations), which would eventually encode much more appropriate information to the end of approximating the Q function. On a similar direction, we propose to combine the unsupervised feature extraction with a supervised feature extraction, aimed at representing some specific information about the environment and its dynamics. When researching the methodology presented in this thesis, we tried to add some features extracted by a CNN trained to approximate the reward function to the feature space, but we only saw a small improvement in performance at the cost of almost doubled runtimes for RFS and FQI. Another example of this could be the pretraining of the encoder on the state dynamics as presented by Anderson et al. (2015) [1]. Moving on to the other components of our learning pipeline, we would also like to expand the work on RFS and FQI.

As we said in Chapter 6, we were not able to properly explore the capabilities of RFS

due to computational limitations. In order to complete the brief tests that we run for this work, we propose to directly compare the performance of the full algorithm using the feature space before and after the selection. This comparison could be the base for a theoretical analysis of the effect of feature selection on deep features. Moreover, a systematic analysis of the actual importance of the features in the representation could lead to better insights on the feature extraction process.

Finally, we think that the batch approach based on FQI could be explored further. Different models, parameters and features could impact greatly on the performance of FQI, even if we were not able to highlight the magnitude of this impact in our tests. Another approach could also change the reinforcement learning component altogether, by moving to a different algorithm like Q-learning while keeping the extraction and selection modules unchanged. A technique like experience replay would also probably help in solving the issue of exploration highlighted in Section 6.5.

Bibliography

[1] Charles W Anderson, Minwoo Lee, and Daniel L Elliott. Faster reinforcement learning after pretraining deep networks to predict state dynamics. In *International Joint Conference on Neural Networks (IJCNN)*, pages 1–7. IEEE, 2015.

[2] Oron Anschel, Nir Baram, and Nahum Shimkin. Averaged-dqn: variance reduction and stabilization for deep reinforcement learning. In *International Conference on Machine Learning (ICML)*, pages 176–185, 2017.

[3] Marc G Bellemare, Yavar Naddaf, Joel Veness, and Michael Bowling. The arcade learning environment: An evaluation platform for general agents. *Journal of Artificial Intelligence Research (JAIR)*, 47:253–279, 2013.

[4] Dimitri P. Bertsekas and John N. Tsitsiklis. Neuro-dynamic programming: an overview. In *IEEE Conference on Decision and Control*, volume 1, pages 560–564. IEEE, 1995.

[5] Christopher M. Bishop. *Pattern recognition and machine learning*. Springer, 2006.

[6] Cameron B. Browne, Edward Powley, Daniel Whitehouse, Simon M. Lucas, Peter I. Cowling, Philipp Rohlfshagen, Stephen Tavener, Diego Perez, Spyridon Samothrakis, and Simon Colton. A survey of monte carlo tree search methods. *IEEE Transactions on Computational Intelligence and AI in games*, 4(1):1–43, 2012.

[7] Murray Campbell, A. Joseph Hoane, and Feng-hsiung Hsu. Deep blue. *Artificial Intelligence*, 134(1-2):57–83, 2002.

[8] Andrea Castelletti, Stefano Galelli, Marcello Restelli, and Rodolfo Soncini-Sessa. Tree-based variable selection for dimensionality reduction of large-scale control systems. In *Adaptive Dynamic Programming And Reinforcement Learning (ADPRL)*, pages 62–69. IEEE, 2011.

[9] John Duchi, Elad Hazan, and Yoram Singer. Adaptive subgradient methods for online learning and stochastic optimization. *Journal of Machine Learning Research (JMLR)*, 12(Jul):2121–2159, 2011.

[10] Dumitru Erhan, Yoshua Bengio, Aaron Courville, Pierre-Antoine Manzagol, Pascal Vincent, and Samy Bengio. Why does unsupervised pre-training help deep learning? *Journal of Machine Learning Research (JMLR)*, 11(Feb):625–660, 2010.

[11] Damien Ernst, Pierre Geurts, and Louis Wehenkel. Tree-based batch mode reinforcement learning. *Journal of Machine Learning Research (JMLR)*, 6(Apr):503–556, 2005.

[12] S. Galelli and A. Castelletti. Tree-based iterative input variable selection for hydrological modeling. *Water Resources Research*, 49(7):4295–4310, 2013.

[13] Sylvain Gelly, Levente Kocsis, Marc Schoenauer, Michele Sebag, David Silver, Csaba Szepesvári, and Olivier Teytaud. The grand challenge of computer go: Monte carlo tree search and extensions. *Communications of the ACM*, 55(3):106–113, 2012.

[14] Pierre Geurts, Damien Ernst, and Louis Wehenkel. Extremely randomized trees. *Machine Learning*, 63(1):3–42, 2006.

[15] Alex Graves, Greg Wayne, and Ivo Danihelka. Neural turing machines. *arXiv preprint arXiv:1410.5401*, 2014.

[16] Alex Graves, Greg Wayne, Malcolm Reynolds, Tim Harley, Ivo Danihelka, Agnieszka Grabska-Barwińska, Sergio Gómez Colmenarejo, Edward Grefenstette, Tiago Ramalho, John Agapiou, AdriÃ Badia, Karl Moritz Hermann, Yori Zwols, Georg Ostrovski, Adam Cain, Helen King, Christopher Summerfield, Phil Blunsom, Koray Kavukcuoglu, and Demis Hassabis. Hybrid computing using a neural network with dynamic external memory. *Nature*, 538(7626):471–476, 2016.

[17] A. Harutyunyan, M. G. Bellemare, T. Stepleton, and R. Munos. Q(λ) with off-policy corrections. In *International Conference on Algorithmic Learning Theory*, pages 305–320. Springer, 2016.

[18] D. Hassabis and D. Silver. Alphago's next move (deepmind.com/blog/alphagos-next-move/), 2017.

[19] Hado V Hasselt. Double q-learning. In *Advances in Neural Information Processing Systems (NIPS)*, pages 2613–2621, 2010.

[20] Hado van Hasselt, Arthur Guez, and David Silver. Deep reinforcement learning with double q-learning. In *AAAI Conference on Artificial Intelligence*, pages 2094–2100. AAAI Press, 2016.

[21] F. S. He, Y. Liu, A. G. Schwing, and J. Peng. Learning to play in a day: Faster deep reinforcement learning by optimality tightening. In *International Conference on Learning Representations (ICLR)*, 2017.

[22] Irina Higgins, Loic Matthey, Arka Pal, Christopher Burgess, Xavier Glorot, Matthew Botvinick, Shakir Mohamed, and Alexander Lerchner. beta-vae: Learning basic visual concepts with a constrained variational framework. In *International Conference on Learning Representations (ICLR)*, 2017.

[23] Irina Higgins, Arka Pal, Andrei Rusu, Loic Matthey, Christopher Burgess, Alexander Pritzel, Matthew Botvinick, Charles Blundell, and Alexander Lerchner. Darla: improving zero-shot transfer in reinforcement learning. In *International Conference on Machine Learning (ICML)*, pages 1480–1490, 2017.

[24] D. P. Kingma and M. Welling. Auto-encoding variational bayes. In *International Conference on Learning Representations (ICLR)*, 2014.

[25] Diederik Kingma and Jimmy Ba. Adam: A method for stochastic optimization. *arXiv preprint arXiv:1412.6980*, 2014.

[26] Alex Krizhevsky, Ilya Sutskever, and Geoffrey E Hinton. Imagenet classification with deep convolutional neural networks. In *Advances in Neural Information Processing Systems (NIPS)*, pages 1097–1105, 2012.

[27] Sascha Lange and Martin Riedmiller. Deep auto-encoder neural networks in reinforcement learning. In *International Joint Conference on Neural Networks (IJCNN)*, pages 1–8. IEEE, 2010.

[28] Yann LeCun, Yoshua Bengio, and Geoffrey Hinton. Deep learning. *Nature*, 521(7553):436–444, 2015.

[29] Long-H Lin. Self-improving reactive agents based on reinforcement learning, planning and teaching. *Machine Learning*, 8(3/4):69–97, 1992.

[30] Jonathan Masci, Ueli Meier, Dan Cireşan, and Jürgen Schmidhuber. Stacked convolutional auto-encoders for hierarchical feature extraction. In *International Conference on Artificial Neural Networks (ICANN)*, pages 52–59, 2011.

[31] Volodymyr Mnih, Adria Puigdomenech Badia, Mehdi Mirza, Alex Graves, Timothy Lillicrap, Tim Harley, David Silver, and Koray Kavukcuoglu. Asynchronous methods for deep reinforcement learning. In *International Conference on Machine Learning (ICML)*, pages 1928–1937, 2016.

[32] Volodymyr Mnih, Koray Kavukcuoglu, David Silver, Andrei A. Rusu, Joel Veness, Marc G. Bellemare, Alex Graves, Martin Riedmiller, Andreas K. Fidjeland, Georg Ostrovski, Stig Petersen, Charles Beattie, Amir Sadik, Ioannis Antonoglou, Helen King, Dharshan Kumaran, Dan Wiestra, Shane Legg, and Demis Hassabis. Human-level control through deep reinforcement learning. *Nature*, 518(7540):529–33, 2015.

[33] R. Munos, T. Stepleton, A. Harutyunyan, and M. Bellemare. Safe and efficient off-policy reinforcement learning. In *Advances in Neural Information Processing Systems (NIPS)*, pages 1054–1062, 2016.

[34] Vinod Nair and Geoffrey E Hinton. Rectified linear units improve restricted boltzmann machines. In *International Conference on Machine Learning (ICML)*, pages 807–814, 2010.

[35] Ian Osband, Charles Blundell, Alexander Pritzel, and Benjamin Van Roy. Deep exploration via bootstrapped dqn. In *Advances in Neural Information Processing Systems (NIPS)*, pages 4026–4034, 2016.

[36] Alexander Pritzel, Benigno Uria, Sriram Srinivasan, Adrià Puigdomènech Badia, Oriol Vinyals, Demis Hassabis, Daan Wierstra, and Charles Blundell. Neural episodic control. In *International Conference on Machine Learning (ICML)*, 2017.

[37] Gavin A. Rummery and Mahesan Niranjan. *On-line Q-learning using connectionist systems*, volume 37. University of Cambridge, Department of Engineering, 1994.

[38] T. Schaul, J. Quan, I. Antonoglou, and D. Silver. Prioritized experience replay. In *International Conference on Learning Representations (ICLR)*, 2016.

[39] David Silver, Aja Huang, Chris J. Maddison, Arthur Guez, Laurent Sifre, George van den Driessche, Julian Schrittwieser, Ioannis Antonoglou, Veda Panneershelvam, Marc Lanctot, Sander Dieleman, Dominik Grewe, John Nham, Nal Kalchbrenner, Ilya Sutskever, Timothy Lillicrap, Madeleine Leach, Koray Kavukcuoglu, Thore Graepel, and Demis Hassabis. Mastering the game of go with deep neural networks and tree search. *Nature*, 529(7587):484–489, 2016.

[40] Karen Simonyan and Andrew Zisserman. Very deep convolutional networks for large-scale image recognition. *CoRR*, abs/1409.1556, 2014.

[41] Richard S. Sutton and Andrew G. Barto. *Reinforcement learning: An introduction*, volume 1. MIT press Cambridge, 1998.

[42] Christian Szegedy, Wei Liu, Yangqing Jia, Pierre Sermanet, Scott Reed, Dragomir Anguelov, Dumitru Erhan, Vincent Vanhoucke, and Andrew Rabinovich. Going deeper with convolutions. In *Computer Vision and Pattern Recognition (CVPR)*, pages 1–9. IEEE, 2015.

[43] Gerald Tesauro. Temporal difference learning and td-gammon. *Communications of the ACM*, 38(3):58–68, 1995.

[44] Aäron van den Oord, Sander Dieleman, Heiga Zen, Karen Simonyan, Oriol Vinyals, Alex Graves, Nal Kalchbrenner, Andrew Senior, and Koray Kavukcuoglu. Wavenet: A generative model for raw audio. In *9th ISCA Speech Synthesis Workshop*, pages 125–125.

[45] Z. Wang, T. Schaul, M. Hessel, H. van Hasselt, M. Lanctot, and N. de Freitas. Dueling network architectures for deep reinforcement learning. In *International Conference on Machine Learning (ICML)*, 2016.

[46] Christopher JCH Watkins and Peter Dayan. Q-learning. *Machine Learning*, 8(3-4):279–292, 1992.

[47] Svante Wold, Kim Esbensen, and Paul Geladi. Principal component analysis. *Chemometrics and Intelligent Laboratory Systems*, 2(1-3):37–52, 1987.

[48] Yonghui Wu, Mike Schuster, Zhifeng Chen, Quoc V. Le, Mohammad Norouzi, Wolfgang Macherey, Maxim Krikun, Yuan Cao, Qin Gao, Klaus Macherey, Jeff Klingner, Apurva Shah, Melvin Johnson, Xiaobing Liu, Lukasz Kaiser, Stephan Gouws, Yoshikiyo Kato, Taku Kudo, Hideto Kazawa, Keith Stevens, George Kurian, Nishant Patil, Wei Wang, Cliff Young, Jason Smith, Jason Riesa, Alex Rudnick, Oriol Vinyals, Greg Corrado, Macduff Hughes, and Jeffrey Dean. Google's neural machine translation system: Bridging the gap between human and machine translation. 2016.

[49] Matthew D. Zeiler. Adadelta: An adaptive learning rate method. *arXiv preprint arXiv:1212.5701*, 2012.

[50] Matthew D. Zeiler, Dilip Krishnan, Graham W. Taylor, and Rob Fergus. Deconvolutional networks. In *Computer Vision and Pattern Recognition (CVPR)*, pages 2528–2535. IEEE, 2010.